



**HAL**  
open science

## Conditions for detection of ground deformation induced by conduit flow and evolution

F. Albino, Virginie Pinel, H. Massol, M. Collombet

► **To cite this version:**

F. Albino, Virginie Pinel, H. Massol, M. Collombet. Conditions for detection of ground deformation induced by conduit flow and evolution. *Journal of Geophysical Research: Solid Earth*, 2011, 116, pp.B06201. 10.1029/2010jb007871 . ird-00607732

**HAL Id: ird-00607732**

**<https://ird.hal.science/ird-00607732>**

Submitted on 11 Jul 2011

**HAL** is a multi-disciplinary open access archive for the deposit and dissemination of scientific research documents, whether they are published or not. The documents may come from teaching and research institutions in France or abroad, or from public or private research centers.

L'archive ouverte pluridisciplinaire **HAL**, est destinée au dépôt et à la diffusion de documents scientifiques de niveau recherche, publiés ou non, émanant des établissements d'enseignement et de recherche français ou étrangers, des laboratoires publics ou privés.

# Conditions for detection of ground deformation induced by conduit flow and evolution

F. Albino<sup>1</sup>, V. Pinel<sup>1</sup>, H. Massol<sup>2</sup> and M. Collombet<sup>1</sup>

---

F. Albino, ISTERre, CNRS, IRD, Université de Savoie, Campus scientifique, 73376 Le Bourget du Lac Cedex, FRANCE. (Fabien.Albino@univ-savoie.fr)

M. Collombet, ISTERre, CNRS, IRD, Université de Savoie, Campus scientifique, 73376 Le Bourget du Lac Cedex, FRANCE.

H. Massol, Laboratoire IDES, Département des Sciences de la Terre, Université Paris XI, 91405 Orsay Cedex, FRANCE.

V. Pinel, ISTERre, CNRS, IRD, Université de Savoie, Campus scientifique, 73376 Le Bourget du Lac Cedex, FRANCE.

<sup>1</sup>ISTERre, CNRS, IRD, Université de Savoie, Campus scientifique, 73376 Le Bourget du Lac Cedex, FRANCE.

<sup>2</sup>Lab. IDES, Département des Sciences de la Terre, Université Paris XI, 91405 Orsay Cedex, FRANCE.

**Abstract.** At mature andesitic volcanoes, magma can reach the surface through the same path for several eruptions thus forming a volcanic conduit. Due to degassing, cooling and crystallization, magma viscosity increase in the upper part of the conduit may induce the formation of a viscous plug. We conducted numerical simulations to quantify the deformation field caused by this plug emplacement and evolution. Stress continuity between Newtonian magma flow and elastic crust is considered. Plug emplacement causes a ground inflation correlated to a decrease of the magma discharge rate. A parametric study shows that surface displacements depend on three dimensionless numbers: the conduit aspect ratio (radius/length), the length ratio between the plug and the conduit and the viscosity contrast between the plug and the magma column. Larger displacements are obtained for high viscosity plugs emplaced in large aspect ratio conduits. We find that only tiltmeters or GPS located close the vent (a few hundred meters) might record the plug emplacement. At immediate proximity of the vent, plug emplacement might even dominate the deformation signal, over dome growth or magma reservoir pressurization effects. For given plug thicknesses and viscosity profiles, our model explain well the amplitude of tilt variations (from 1 to 25  $\mu rad$ ) measured at Montserrat and Mt. St. Helens. We also demonstrate that, at Montserrat, even if most of the tilt signal is due to shear stress induced by magma flow, pressurization beneath the plug account for 20 percent of the signal.

## 1. Introduction

1 Cyclic patterns of activity, with a succession of episodes of lava dome growth and  
2 quiescent periods, have been observed at many andesitic volcanoes, such as Soufrière Hills  
3 (Montserrat, 1995-present), Mt St Helens (USA, 1980-1986), Merapi (Philippines, 1768-  
4 1998), Unzen (Japan, 1990-1995) or Santiaguito (Guatemala, 1922-2000) [Voight *et al.*,  
5 1999; Swanson and Holcomb, 1990; Voight *et al.*, 2000; Nakada *et al.*, 1999; Harris *et al.*,  
6 2002]. Large fluctuations in discharge rate are correlated with fluctuations of various  
7 signals such as ground deformation, seismicity and gas emissions. For long-term cycles,  
8 (months to years), the mechanism invoked is pressure changes occurring within a magma  
9 reservoir [Melnik and Sparks, 2005]. In some volcanic areas such as Soufrière Hills, Mt St  
10 Helens or Merapi, improvement of volcanic monitoring, with acquisitions of high frequency  
11 and precise data, has permitted to identify cyclic patterns with a period of only a few  
12 hours, during phases of dome extrusion [Voight *et al.*, 1999]. Whereas cyclic deformation  
13 at long time-scales is attributed to magma reservoir dynamics, short time-scale variations  
14 are explained by the non-linear dynamics of magma flow in the volcanic conduit [Denlinger  
15 and Hoblitt, 1999; Voight *et al.*, 1999; Wylie *et al.*, 1999; Lensky *et al.*, 2008; Collier and  
16 Neuberg, 2006]. Intermediate cycles with periods of several weeks have been attributed  
17 to the capacitor effect of dykes connecting magma reservoirs and upper conduits [Costa  
18 *et al.*, 2007b]. Also, sudden events characteristic of andesitic volcanic activity, such as  
19 dome collapse, can induce rapid pressure changes within the magma reservoir [Voight  
20 *et al.*, 2006]. It follows that a combination of changes taking place at different levels of  
21 the magma plumbing system, causes the temporal evolution of volcanic activity. In order

22 to improve eruption forecasting, it is required to study magma flow conditions in the  
23 volcanic conduit of andesitic volcanoes and how it affects the monitoring signals recorded  
24 at the surface.

25 Previous work [*Sparks, 1997; Melnik and Sparks, 1999; Barmin et al., 2002*], focussing  
26 on changes of the physical properties of the ascending magma, has shown that gas loss  
27 and crystallization occur mainly within the last hundred of meters below the surface.  
28 Both mechanisms may induce a strong increase in magma viscosity of several orders  
29 of magnitude [*Shaw, 1963; Hess and Dingwell, 1996; Llewellyn and Manga, 2005*]. For  
30 example, the viscosity of an andesitic magma at 900 °C containing 5 wt% is around  $10^4$   
31 Pa.s, but can reach values of  $10^{11}$  Pa.s if the magma is fully degassed [*Sparks, 1997*]. In this  
32 process, vertical as well as lateral gas escape may have a strong impact on the resulting  
33 viscosity profiles [*Collombet, 2009*]. It has been shown that degassing may be coupled with  
34 crystallization which, in turn, also affects magma viscosity [*Sparks, 1997*]. *Costa et al.*  
35 [2007a] consider a strong dependency of the viscosity on crystal content, with an increase  
36 in crystal content from 50 to 80 vol % leading to an increase in viscosity by a factor of  
37  $10^8$ . As a consequence of these shallow crystallization and degassing processes, a more  
38 viscous body, so-called plug, is typically emplaced at the upper part of the conduit. The  
39 presence of this degassed portion in the upper part of the conduit has been confirmed by  
40 petrological studies performed on explosive deposits at Soufrière Hills Volcano, Montserrat  
41 [*Burgisser et al., 2010*]. The plug formation tends to reduce the magma flow rate and also  
42 induces a pressurization within the conduit. Changes in magma rheology modify the  
43 overall flow dynamics within the conduit and, consequently, the stress field within the  
44 surrounding crust, which might therefore induce precursor signals such as deformation

45 or seismicity. Ground deformation related to conduit flow processes has been studied  
46 through analytic solutions [*Bonaccorso and Davis, 1999; Nishimura, 2006, 2009*] as well  
47 as numerical modelling [*Chadwick et al., 1988; Beauducel et al., 2000; Green et al., 2006;*  
48 *Hautmann et al., 2009*]. However, deformation of the conduit wall due to the magma flow  
49 was not taken into consideration and most of studies considered only one component of  
50 the stress field acting on the wall rocks, either shear stress [*Beauducel et al., 2000; Green*  
51 *et al., 2006*] or normal stress [*Hautmann et al., 2009*]. Only few studies consider both  
52 components [*Chadwick et al., 1988; Anderson et al., 2010*]. However, in these studies, the  
53 two effects are evaluated independently despite their obvious link through flow motion  
54 equations [*Nishimura, 2009*].

55 Here, we consider the full coupling between the fluid flow and crustal deformation, taking  
56 into account the total stress field and the deformation of the conduit wall. We carry out  
57 numerical calculations in axial geometry to model the displacement field induced by a  
58 steady flow when a plug is emplaced at the top of the conduit. We perform a parametric  
59 study in order to quantify the deformation field induced by the increase of magma viscosity  
60 at the upper part of the conduit and give an estimation of the distance of detection of  
61 the induced signal. We then compare the magma flow rate and the surface tilt expected  
62 during plug growth within the conduit. We further discuss our results with regards to  
63 data recorded at the two most studied andesitic volcanoes, Soufrière Hills (Montserrat)  
64 and Mount St Helens (USA), and consider more realistic flow conditions as well as data  
65 acquisition geometry (including volcano topography).

## 2. Model

### 2.1. Description

66 Magma flow through a volcanic conduit embedded in the crust is modelled using a  
67 "Finite Element Method" (FEM) in axisymmetrical geometry (COMSOL software). The  
68 conduit is a vertical cylinder with radius ( $a_c$ ) and length ( $L_c$ ). The magma, considered as  
69 a Newtonian fluid, flows with steady state conditions due to an overpressure ( $P_c$ ), which  
70 is an excess of pressure comparing to the lithostatic state, applied at the conduit bottom.  
71 This excess pressure is due to the presence of an overpressurized storage zone, which effect  
72 is not modeled in the present study. Our model is not time dependent and describes  
73 the departure induced by a given steady state magma flow within the conduit, from a  
74 reference state being a lithostatic state of stress within the surrounding rocks with an  
75 overpressurized reservoir not connected to the surface. It means that all the displacement  
76 and state of stress calculated are the one induced by the magma flow within the conduit.  
77 The surrounding crust is treated as a homogeneous elastic medium, characterized by its  
78 shear modulus ( $G$ ) which will be variable and its Poisson's ratio ( $\nu$ ) which is fixed at 0.25  
79 in all our study. Boundary conditions used for the host rock medium are the following  
80 (see Figure 1): (i) free displacements at the top boundary, which corresponds to the  
81 ground surface ; (ii) no vertical displacement at the bottom boundary and (iii) no radial  
82 displacement at the external lateral boundary. In order to neglect the boundary effects,  
83 the external lateral boundary of the elastic medium is located far away from the conduit  
84 (at a distance of 100 km). A full coupling of magma flow and crustal deformation is  
85 considered by applying the continuity of the stress field (Fig. 1), including normal as well  
86 as tangential components, at the conduit wall. Conduit wall deformation is calculated

87 by an iterative process as described in Appendix A. Geometry, physical properties and  
 88 boundary conditions applied in our model are shown in Figure 1a.

89 The steady state of fluid flow is solved from the Navier & Stokes equation. A complete  
 90 parametric study is performed for an incompressible fluid with a constant density ( $\rho_m$ )  
 91 equal to the surrounding crustal density, a viscosity function ( $\mu(z)$ ) and characterized by  
 92 a Poiseuille flow. We later consider in the discussion a compressible fluid associated to  
 93 complex and realistic flow conditions. In the incompressible case, the component of the  
 94 stress normal to the conduit wall is equal to the magma pressure. We first calculate per-  
 95 turbations of the reference state induced by the flow of a constant viscosity magma. This  
 96 solution is then considered as our new state of reference. We then quantify displacements  
 97 induced by the emplacement of a more viscous portion of the flow, so-called plug, at the  
 98 top of the conduit with respect to the constant viscosity case.

99 To first order, the increase of viscosity is approximated by a step function (Fig. 1b)  
 100 that is dependent on the conduit depth. The plug is characterized by two parameters:  
 101 its viscosity ( $\mu_p$ ), with  $\mu_p > \mu_m$  ( $\mu_m$  being the viscosity of the magma column) and its  
 102 length ( $h_p$ ), with  $h_p < \frac{1}{2}L_c$ . For Poiseuille flow, with a constant viscosity, expressions  
 103 for the stress field components at the conduit walls are simplified: (i) the normal stress  
 104 is equivalent to the fluid pressure and varies linearly with depth,  $\frac{dP}{dz} = cste$ ; (ii) the  
 105 tangential stress or shear stress is a constant value, which only depends on the pressure  
 106 gradient and the conduit radius,  $\tau = (\frac{a_c}{2})(\frac{dP}{dz}) = cste$ . In that case, and providing  
 107 that the conduit deformation remains small (see Appendix A for conditions), we solve  
 108 equations for the stress and displacement field within the elastic medium, applying the  
 109 stress components corresponding to the fluid flow at the conduit wall. For magmas with

constant viscosity (our reference case), the pressure gradient as well as the tangential stress applied at the conduit wall are constant  $\tau_{ref} = \frac{a_c P_c}{2L_c}$  (the dashed curve on Fig. 1b). In this case, for a given Poisson's ratio, the surface displacements are a function of the conduit geometry ( $a_c$ ,  $L_c$ ), the overpressure at the bottom of the conduit ( $P_c$ ) and the shear modulus ( $G$ ) only. They do not depend on the viscosity value. For a plug model, the tangential stress is different from the reference case both at the upper part of the conduit ( $\tau_{up}$ ) and at the lower portion ( $\tau_{low}$ ) (solid curve in Fig. 1b). The increase of magma viscosity within the upper part induces an overpressure when compared to the reference case (of constant viscosity). This overpressure reaches a maximum value, denoted  $\Delta P_p$ , at the base of the plug (Fig. 1b). At the plug bottom, the magma pressure,  $P_p$ , can be derived using the conservation of the volumetric flux along the conduit:

$$P_p = \frac{\mu_p h_p}{\mu_p h_p + \mu_m (L_c - h_p)} P_c \quad (1)$$

where  $P_c$  is the excess pressure at the conduit bottom. It follows that the overpressure ( $\Delta P_p$ ) can be expressed as a function of the viscosity contrast and the length ratio:

$$\Delta P_p = P_p - \frac{h_p}{L_c} P_c = \left( \frac{\left(\frac{\mu_p}{\mu_m}\right)\left(\frac{h_p}{L_c}\right)}{1 + \frac{h_p}{L_c}\left(\frac{\mu_p}{\mu_m} - 1\right)} - \frac{h_p}{L_c} \right) P_c \quad (2)$$

This overpressure is equal to zero when there is no viscosity contrast,  $\mu_p = \mu_m$ , and reaches the value  $P_c(1 - \frac{h_p}{L_c})$  when the viscosity within the plug tends to infinity. For the plug case, the two magma viscosities,  $\mu_m$  and  $\mu_p$ , as well as the length of the plug,  $h_p$ , have an effect on the displacement. For a given Poisson's ratio and using the conduit length ( $L_c$ ) as a length scale and the term  $(\frac{P_c}{G} L_c)$  as a displacement scale, dimensionless solutions are only dependent on the following three dimensionless numbers: (i) the conduit aspect ratio

131  $(\frac{a_c}{L_c})$ , (ii) the length ratio between the plug and the total conduit  $(\frac{h_p}{L_c})$ , (iii) the viscosity  
132 ratio between the two magmas  $(\frac{\mu_p}{\mu_m})$ .

## 2.2. Main Limitations

133 Our model should be taken as a first attempt to link surface deformation as well as  
134 magma flow rate evolution to main characteristics of the magma properties evolution  
135 within its upper path to the Earth's surface. Here, we do not intent to solve the whole flow  
136 complexity but rather to couple a simple but coherent stress state with the deformation  
137 of the surrounding rocks. As a consequence our model contains a number of assumptions  
138 which have to be discussed. It is, however, noteworthy that many of these limitations  
139 could be reduced in further developments of the model.

140 The first assumption is the choice of a cylinder geometry to model the volcanic conduit.  
141 Magma, usually stored in a shallow reservoir, is connected to the surface through a crustal  
142 pathway. Dyke propagation is considered as the main mechanism which can initiate the  
143 pathway through the crust at deep level from the magma storage zone [Lister and Kerr,  
144 1991; Rubin, 1995] and there are geological as well as geophysical evidences of the feeding  
145 of lava domes by dykes [Mastin and Pollard, 1988; Nakada and Eichelberger, 2004; Roman  
146 *et al.*, 2006]. However, for many andesitic volcanoes, such as Mt Usu (Japan), Soufrière  
147 Hills (Montserrat), Santiaguito (Guatemala) and Mt. St. Helens (USA), cylindrical con-  
148 duits can develop during lava dome eruptions [Yokoyama, 1981; Sparks and Young, 2002;  
149 Williams and Self, 1983; Swanson and Holcomb, 1990]. Evidence of the existence of  
150 cylindrical conduit is supported by observations of the geometry of the crater vents and  
151 extruded bodies ("spine") during dome growth [Sparks and Young, 2002; Iverson *et al.*,  
152 2006]. This particular shape is formed during explosive eruptions which frequently occurs

153 before extrusive activity. One of the consequence is that the cylinder conduit is prob-  
154 ably limited to the last hundred meters, but it can reach several kilometers in case of  
155 high fragmentation and large depressurization. The extension at depth of this cylindrical  
156 shape is still under debate. Some authors suggest a possible connection between a shallow  
157 cylindrical conduit and a deep dyke [*Costa et al.*, 2007b, a]. The effect of the pressurized  
158 dyke as well as a pressurized magma reservoir below the cylindrical conduit will act on  
159 magma flux and also on ground deformation on large time scale, over weeks to year. Here,  
160 we are interested in the short time scale deformation only occurring during rapid changes  
161 in magma flow dynamics at shallow level. In consequence, our model only focus on the  
162 shallow part of a mature magmatic system associated to cylindrical shapes, which has  
163 already been considered in many studies in relation with conduit flow [*Wylie et al.*, 1999;  
164 *Melnik and Sparks*, 1999; *Barmin et al.*, 2002; *Collier and Neuberg*, 2006; *Lensky et al.*,  
165 2008; *Collombet*, 2009].

166 The second main assumption of our model is the choice of a Newtonian behaviour for  
167 the magma. Indeed, different processes, such as magma crystallization and cooling or high  
168 volatile contents may lead to a non-Newtonian behaviour, implying a dependence of the  
169 viscosity with the shear rate. The non-Newtonian behaviour is reached for high crystal-  
170 bearing magmas, containing more than 30-40% of crystals [*Pinkerton and Stevenson*,  
171 1992; *Lejeune and Richet*, 1995]. This threshold can be reached in the case of Soufrière  
172 Hills [*Sparks et al.*, 2000] or Mt. St Helens [*Gardner et al.*, 1996] volcanoes if the andesitic  
173 magmas spend a significant duration in the conduit. Recent publications, such as [*Caricchi*  
174 *et al.*, 2007] show that, the magma behaviour is also highly dependent on the strain rate  
175 considered and for high values (above  $10^{-4} \text{ s}^{-1}$ ) magma overall viscosity decreases with

176 strain rates exhibiting non-Newtonian behaviour. In that case, the velocity profile should  
177 departs from the Poiseuille parabolic profile affecting values of the shear stress at the  
178 conduit wall. Considering Figure 3 from *Caricchi et al.* [2007] we can predict that the  
179 shear stress may decrease of approximately one order of magnitude comparing with the  
180 Newtonian case.

181 Another strong limitation of our model comes from the fact that thermal effects are not  
182 taken into account. However they could potentially favor non-Newtonian behaviour of the  
183 magma as well as affect stresses applied at the conduit wall. During ascent of hot magma in  
184 a cold crust, large thermal gradient can develop at the conduit wall. Mechanism of magma  
185 cooling or host rocks heating due to viscous effect can occur and the dominant effect  
186 depends on the flow conditions [*Costa et al.*, 2007c]. For example, a thermal boundary  
187 layer due to cooling effect should represent less than 0.5 m of the conduit radius and leads  
188 to a decrease of 100 to 200 K of temperature [*Collier and Neuberg*, 2006]. In opposite  
189 way, viscous heating effects can produce an increase of temperature at the wall and induce  
190 changes in the velocity profile of the flow, which evolves from parabolic (as we consider  
191 in our paper) to plug-like [*Costa and Macedonio*, 2005; *Costa et al.*, 2007c]. But these  
192 variations in temperature near the wall implies a melt viscosity change of one order of  
193 magnitude [*Hess and Dingwell*, 1996], which is much less than viscosity changes due to  
194 gas loss during magma ascent [*Sparks*, 1997]. In consequence, we believe that, despite  
195 this simplification, we capture the first order effect in our model.

### 3. Results

#### 3.1. Surface Displacements

196 In this section, we explore a range of parameters for each dimensionless number to  
 197 describe the influence of various parameters on the ground deformation. In each model,  
 198 radial ( $U_r$ ), vertical ( $U_z$ ) displacements and tilt ( $\frac{\delta U_z}{\delta r}$ ) at the surface are calculated. Radial  
 199 and vertical displacements are positive when directed, respectively, outward and up from  
 200 the conduit wall (see r,z direction in Fig. 1a). Tilts are negative when the surface is  
 201 moving upward going toward the vent, which corresponds to a ground inflation. For all  
 202 calculations, the Poisson's ratio value is 0.25. Results for the reference state (i.e. constant  
 203 viscosity:  $\frac{\mu_p}{\mu_m} = 1$ ) for three different conduit aspect ratios ( $\frac{a_c}{L_c}$ ) are shown in Figure 3.  
 204 The displacement trend is similar for various conduit aspect ratios except in the vicinity  
 205 of the vent where differences are observed for radial distances less than 20% of the conduit  
 206 length. The amplitude of the displacements and tilts is more important for larger values of  
 207  $\frac{a_c}{L_c}$ , corresponding to the largest or shortest conduits. This means, as previously shown by  
 208 *Chadwick et al.* [1988], that a larger pressure is required to explain a given displacement  
 209 when considering a smaller conduit radius. In Figure 3, we also show that displacements  
 210 are both induced by the shear stress component and by the pressure. Both components  
 211 induce displacements of the same order of amplitude. For radial displacements, shear  
 212 stress has a strong influence in the near field (for  $\frac{r}{L_c} < 0.5$ ) whereas pressure has more  
 213 effect in the far field (for  $\frac{r}{L_c} > 0.5$ ). For vertical displacements and tilts, pressure and shear  
 214 stress induce opposite ground movement. Shear stress induces inflation whereas pressure  
 215 induces deflation. However, the amplitude of the shear stress effect is larger, which results  
 216 in a total displacement directed upward. In this case, neglecting the pressure component

217 leads to an overestimate in the induced displacement field. For near field measurements,  
 218 this overestimation is larger for a smaller conduit aspect ratio ( $\frac{a_c}{L_c}$ ). For example, our  
 219 model gives an overestimation, larger than 20% for the tilt at a distance of 500 m from the  
 220 conduit, if pressure at the conduit wall is neglected, with the conditions taken by *Green*  
 221 *et al.* [2006] to model tilt recorded at Montserrat volcano (i.e.: a shear stress of 0.5 MPa  
 222 applied on the wall of a conduit with a 1000 m length and a 15 m radius and a Young's  
 223 modulus fixed at 2 GPa). Thus, each stress component has an important effect on the  
 224 total displacement field and none of them should be neglected in deformation models.

225 In case a viscous plug is present at the top of the conduit, displacements larger than  
 226 those described above, for the constant viscosity case, are induced. We calculate surface  
 227 tilts due to plug flow models exploring the range of  $10^0$ - $10^5$  for the viscosity ratio ( $\frac{\mu_p}{\mu_m}$ )  
 228 and 0-0.5 for the length ratio ( $\frac{h_p}{L_c}$ ). Figure 4 shows the tilts calculated at a radial distance  
 229 of 500 m from the conduit, for the tested parameter range, considering a conduit of 15 m  
 230 radius and 5000 m length. Magma pressure at the conduit bottom ( $P_c$ ) and the elastic  
 231 shear modulus ( $G$ ) of the crust are respectively fixed at 10 MPa and 0.8 GPa. Such values  
 232 seem realistic for Soufrière Hills [*Green et al.*, 2006; *Costa et al.*, 2007b; *Voight et al.*, 1999].  
 233 Tilt calculation is relative to our reference case obtained with constant viscosity, such that  
 234 it's value tends to zero when either  $h_p$  tends to zero or  $\frac{\mu_p}{\mu_m}$  tends to 1. Figure 4a shows  
 235 that the plug emplacement induces an inflation (negative tilt values). At 500 m from the  
 236 conduit wall, tilt values reach more than 3  $\mu rad$  for thin plugs characterized by a large  
 237 viscosity contrast ( $\frac{\mu_p}{\mu_m} > 10^{2.5}$  and  $\frac{h_p}{L_c} < 0.05$ ). However the largest displacements are  
 238 not always obtained with the thinnest plugs: for small viscosity ratios ( $\frac{\mu_p}{\mu_m} < 10^3$ ), there  
 239 exists a critical plug thickness,  $h_{p(crit)}$ , corresponding to a maximum of the induced tilt

240 amplitude. For large viscosity ratios ( $\frac{\mu_p}{\mu_m} > 10^3$ ),  $h_{p(crit)}$  tends to zero: the tilt increases  
241 when the plug length decreases. In addition, for large viscosity ratio, tilt does not depend  
242 on the viscosity ratio, but is mainly a function of the plug length. The influence of each  
243 stress component on the ground displacements is also shown in Figure 4b and 4c. Even  
244 if the pressure acting along the conduit wall does not dominate the tilt signal, it has a  
245 strong influence inducing a ground deflation (positive tilt values). The effect is maximum,  
246 with an amplitude larger than 1  $\mu rad$ , for intermediate length ratios (between 0.1 and  
247 0.3). In most cases, except for the thinnest plugs, neglecting the pressure effect leads to  
248 overestimate the induced tilt, which means that the tangential stress component will be  
249 underestimated when interpreting an observed signal.

### 3.2. Detection of Ground Deformation

250 We have showed that an increase of magma viscosity occurring at the top of a conduit,  
251 increases tilts at the ground surface. In order to guide the choice for in-situ instru-  
252 ment types and locations, it seems important to quantify the maximal distance from  
253 the volcanic vent, where this signal can be detected. We estimate this critical distance,  
254 hereafter called "detection distance" using a threshold value of detection for each com-  
255 ponent of the displacement. Horizontal and vertical ground movements can be detected  
256 by GPS receivers. The theoretical precision of the instrumentation used in volcanology  
257 is around 5 mm and 10 mm respectively for the horizontal and vertical displacement  
258 (<http://www.igage.com/GPSaccy/index.html>). However, field measurements can be per-  
259 turbed by the atmospheric component or local perturbations of the instrumented site. We  
260 thus assume in our study that only millimetric changes for the radial displacements and  
261 centimetric changes for the vertical displacements will be detected. On the other hand,

262 a more accurate method to detect ground motion is to measure the tilt of the volcano  
263 surface. According to the tiltmeters used, ground deformation less than  $1 \mu rad$  can be  
264 detected (<http://www.carboceramics.com/Tiltmeters-Clinometers>), one microradian cor-  
265 responding to a vertical variation of one millimeter over a distance of one kilometer. This  
266 type of measurement is difficult to set up because instruments are highly sensitive to  
267 changes in temperature or atmospheric pressure. In order to minimize the influence of  
268 these external effects on recorded measurements, tiltmeters are often placed in boreholes,  
269 several centimeters beneath the surface. Here, we choose an upper value for our detection  
270 threshold and we consider that only tilt variations larger than  $1 \mu rad$  are detected.

271 We use the same model parameters as in Figure 4 ( $G = 0.8$  GPa,  $\nu = 0.25$ ,  $P_c = 10$   
272 MPa,  $L_c = 5000$  m and  $a_c = 15$  m) and threshold values of 1 mm and 1 cm respectively  
273 for the radial and the vertical displacements, and  $1 \mu rad$  for the tilt. We find that: (i)  
274 radial displacement is never detectable for plugs representing more than 20% of the total  
275 conduit, but it can be observed over 1 km for plugs with length ratio less than 10% and  
276 viscosity contrast more than  $10^2$  (see figure 5a). (ii) vertical displacement can never be  
277 detected, except a few meters from the conduit for the thinnest plugs (see figure 5b).  
278 (iii) tilt can be detected for a few hundred meters depending on the plug characteristics  
279 as detailed in Figure 6c. Tiltmeters or GPS located at a few hundred meters from the  
280 conduit are thus appropriate to detect the ground deformation, respectively tilt or radial  
281 displacement, induced by plug emplacement within the upper part of a volcanic conduit.  
282 As previously explained, the amplitude of the displacements is not only dependent on the  
283 viscosity ratio ( $\frac{\mu_p}{\mu_m}$ ) and length ratio ( $\frac{h_p}{L_c}$ ) but is also function of the balance between  
284 the reservoir overpressure and the host rocks elastic properties,  $\frac{P_c}{G}$ , as well as the conduit

285 aspect ratio ( $\frac{a_c}{L_c}$ ). Figure 6 shows the effect of these two parameters on the detection  
 286 distance. The case c) is calculated for a radius  $a_c$  equal to 15 m and a shear modulus  
 287  $G$  equal to 0.8 GPa, values previously used. The case a) provides the detection distance  
 288 for a larger radius ( $a_c$ ), the case d) for a larger shear modulus ( $G$ ) and the case b)  
 289 when both parameters are increased. As expected, an increase of the conduit radius or a  
 290 decrease of the host rocks shear modulus, tends to increase the detection distance for tilt  
 291 signal. During the extrusive phase, the detection of ground deformation caused by plug  
 292 emplacement will be much easier in the case of andesitic volcanoes with a large conduit  
 293 embedded in soft host rocks.

### 3.3. Flow Rate Versus Tilt Signal During Plug Evolution

294 The formation of a viscous plug at the top of the volcanic conduit induces a decrease  
 295 of magma flow. The flow rate for a plug model can be expressed as a function of the  
 296 reference flow rate,  $Q_{ref}$ , of the "constant viscosity" case:

$$297 \quad Q = \left( \frac{1}{1 + \frac{h_p}{L_c} (\frac{\mu_p}{\mu_m} - 1)} \right) Q_{ref} \quad (3)$$

298 In the previous section, we showed that plug emplacement also induces ground motion  
 299 signals large enough to be detected under certain conditions. During the extrusive phases  
 300 of andesitic volcanoes, a plug may form in the upper portion of the conduit and evolve  
 301 through time due to continuous degassing as well as cooling and crystallization processes.  
 302 Plug evolution can proceed either through an increase of its viscosity or its size. In nature,  
 303 both cases are probably mixed, but here we choose to compare the relative evolution of  
 304 tilt and flow rates observed at the surface as a consequence of these two end-members  
 305 (Figure 7).

306 For a given plug length, an increase of plug viscosity reduces, as expected, the magma  
307 flow rate produced at the surface (Fig. 7b, left panel). As a consequence of this flow rate  
308 decrease, the amount of time required to entirely extrudes the plug considered (thickness  
309  $h_p$  and viscosity  $\mu_p$ ), increases (Fig. 7c, left panel). This duration corresponds to the  
310 expected duration of the deflation induced by the plug extrusion. Whatever the value  
311 of  $\frac{h_p}{L_c}$ , the flow rate falls below 5% of its reference value for a viscosity contrast larger  
312 than  $10^3$ . This increase of viscosity induces a ground inflation: the tilt amplitude first  
313 increases with the viscosity contrast before reaching a constant and maximum value (Fig.  
314 7a, left panel). The threshold value of viscosity at which the maximum of tilt amplitude  
315 is reached, depends on the plug size, with larger values for thinner plugs. For plugs that  
316 are more viscous than the threshold value, the tilt amplitude remains constant and the  
317 magma flow rate is close to zero. Thus, if a high contrast of viscosity already exists  
318 between the plug and the magma column, the evolution of the plug viscosity can not be  
319 detected from the surface displacement measurements.

320 The other end-member behaviour is the one induced by a thickening plug of constant  
321 viscosity. Once again due to plug evolution, the magma flow rate decreases (Fig. 7b, right  
322 panel) and the extrusion duration consequently increases (Fig. 7c, right panel). However  
323 for small viscosity contrasts, the flow rate reduction remains small. For the induced tilt  
324 (Fig. 7a, right panel), the behaviour is different than in the previous case: we observe  
325 a rapid ground inflation (upward displacement when going towards the crater), until the  
326 plug reaches its critical thickness,  $h_{p(crit)}$ , as previously defined. Once the plug thickness  
327 is larger than this critical value, the tilt amplitude decreases together with the flow rate.  
328 For a large viscosity contrast, the critical thickness tends to zero, and the first phase can

329 not be distinguished. This result is related to the fact that the maximum amplitude of the  
330 surface tilts is not always obtained for the thinnest plugs but for a critical plug size, which  
331 depends on the viscosity contrast. For plugs larger than the critical thickness, the decrease  
332 trend of the tilt amplitude is mainly controlled by the variation of the pressurization level  
333 ( $h_p$ ) rather than its value ( $\Delta P_p$ ). Indeed, an increase of the plug length corresponds to  
334 an increase of the depth of the maximal pressurization within the conduit.

335 To summarize, in the early stage of plug emplacement (a small viscosity contrast and  
336 a thin thickness), the resulting increase of overpressure due to the plug,  $\Delta P_p$ , induces an  
337 inflation, while the magma flow rate is reduced. Depending on the preponderant effect  
338 during plug growth, either in the thickness or in the viscosity contrast evolution, an  
339 increase or a decrease of tilt amplitude might occur afterward. The joint interpretation  
340 of the flow rate and ground motion evolution through time, using this kind of model, can  
341 thus provide useful constrains on magma viscosity profiles within the conduit. Tracking  
342 the evolution of magma physical properties through time is essential to explain drastic  
343 and sudden changes of magmatic activity observed at andesitic volcanoes.

## 4. Discussion

### 4.1. Effect of Conduit Flow Versus Other Deformation Sources

344 In this study, we have modelled ground motion due to magma conduit flow considering  
345 no pressure changes within the magma reservoir and no magma accumulation at the  
346 surface. It is obvious, however, that flow dynamics changes occurring within the conduit  
347 are not the only source of deformation on andesitic strato-volcanoes. Pressure changes  
348 within a shallow magma reservoir [*Mogi, 1958*] and surface load variations due to dome  
349 growth/collapse can also induce ground motion [*Beauducel et al., 2000*]. Figure 8 allows a

350 comparison of the relative amplitude of these various phenomena. It shows displacements  
351 induced by (i) surface pressure change of 1 MPa related to the emplacement/removal  
352 of a lava dome (1 MPa corresponding to a height change of 60 m of a material with  
353 a density of  $1700 \text{ kg.m}^{-3}$ ), (ii) an overpressure variation of 1 MPa occurring within a  
354 magma reservoir and (iii) the emplacement of a plug in the upper part of the conduit.  
355 All the parameters taken for these models are detailed in the caption of the Figure 8.  
356 In the far field, at distances greater than  $0.2 L_c$  from the volcanic vent, magma pressure  
357 changes or dome height variations induce larger displacements at the Earth's surface than  
358 the magma conduit flow. Emplacement of a plug at the top of the conduit might induce  
359 larger amplitudes than magma reservoir or lava dome processes, in radial displacements  
360 as well as in tilt signal, only in the immediate vicinity of the vent.

361 To conclude, with the context of an incompressible magma, ground motion induced by  
362 magma viscosity increases at the top of the volcanic conduit will be detectable only if: (i)  
363 instruments are located in the near field, few hundred meters from the volcanic vent ; (ii)  
364 plugs have reduced size and high viscosity contrast compared to the magma column ; (iii)  
365 other processes, such as magma reservoir pressure changes or lava dome growth/collapse,  
366 do not dominate the deformation signal. *Melnik and Sparks* [2005] proposed a transient  
367 model of magma flow in an open volcanic conduit including gas exsolution and escape,  
368 bubble growth as well as crystallization effects. They show that the system can fluctuate  
369 between two stable states, one being characterised by a high flow rate of less viscous  
370 magma and the other by a low flow rate of more viscous magma. Considering the given  
371 viscosity profiles and reservoir overpressures, we have quantified the induced displacements  
372 when the system goes from one regime to the other. Deformation at the surface is almost

373 entirely due to the pressure changes occurring within the reservoir, the viscosity profile  
374 changes occurring within the conduit having a smaller effect. However the model proposed  
375 by *Melnik and Sparks* [2005] cannot simultaneously explain cycles occurring on a period of  
376 several years or several weeks. Short time-scales cycles have been explained by models with  
377 a constant reservoir pressure [*Costa et al.*, 2007b], which justifies our choice to quantify  
378 the displacement field induced by magma flow condition within the conduit in case there  
379 is no magma reservoir pressure change.

380 Conversely, the fact that conduit effects might dominate the deformation signal in the  
381 immediate vicinity of the vent, implies the necessity to have some distant instruments in  
382 order to monitor magma pressure changes within storage zones.

## 4.2. Influence of Topography

383 In all previous calculations, the volcano surface is modelled as a flat surface, but an-  
384 desitic strato-volcanoes are characterized by significant topography with slopes up to 35°.  
385 Because topography can have an effect on ground deformation results [*Cayol and Cornet*,  
386 1998], we calculated tilts induced by plug emplacement with an upper surface correspond-  
387 ing, in the first approximation (a linear trend), to Montserrat topography. Including this  
388 topography, we obtained the same conclusions as for a flat topography,

## 4.3. Influence of Viscosity Profile

389 At Soufrière Hills Volcano (Montserrat), tilt cycles were recorded at 600-700 m from  
390 the crater vent, first in December 1996 with an amplitude of 1-2  $\mu rad$  and a period of 6-8  
391 h, and few months after, from April to May 1997, with an amplitude between 10 and 25  
392  $\mu rad$  and a period of 12-18 h [*Voight et al.*, 1998]. The cyclic behaviour of the surface

393 deformation, with a deflation phase more rapid than the inflation one, is also correlated  
394 with cycles in seismic activity and gas emissions of  $\text{SO}_2$  [Watson *et al.*, 2000]. At Mt  
395 St Helens, variations of the tilt amplitude were also measured during the active period  
396 between the years 2004 and 2008 by *Anderson et al.* [2010]. Tiltmeters, located within  
397 the crater and close the dome (around 150-250 m from the vent), recorded many cyclic  
398 tilt events characterized by a duration from minutes to hours and a mean amplitude close  
399 to  $1 \mu\text{rad}$ . The pattern of the cycle begin with, a rapid inflation (outward tilt) followed  
400 by a gradual subsidence (inward tilt). Here, we compare the amplitude of tilt recorded at  
401 Montserrat and Mt St Helens with those obtained by our plug models (Fig. 9b). Assuming  
402 a value of 0.8 GPa for the shear modulus, 0.25 for the Poisson's ratio and 10 MPa for  
403 the magma reservoir overpressure, a high viscous plug emplaced in the upper part of the  
404 conduit can produce the amplitude of tilt cycles recorded at both volcanoes. At Mt St  
405 Helens, surface tilt induced by a plug occupying 25 % of the conduit fits the data collected  
406 during the period July 1996-January 1997. In the same way, at Soufrière Hills, a plug  
407 emplaced in the upper 10 % of the conduit can also explain the tilt data recorded during  
408 December 1996. However, our plug models cannot produce the large tilt amplitude of  
409  $10\text{-}25 \mu\text{rad}$  measured during the April-May 1997 at Montserrat. In our model, we always  
410 assumed that viscosity increase at the top of the conduit follows a step function and we  
411 consider that the magma density is constant over the conduit. But, this viscosity profile is  
412 simplified and magma density also evolves with depth. To overcome this simplification, we  
413 also calculated tilt induced by other flow models considering realistic viscosity profiles, and  
414 compare to results previously obtained with our plug model. The first one is taken from  
415 *Sparks* [1997] and corresponds to the model 3 presented in the paper as a case "where

416 a lava dome up to 100 m thick is being fed from a conduit and the gas is lost during  
417 ascent for magma that just remains gas-saturated at the local pressure”. In this model,  
418 the viscosity profile is expressed as a power law of the depth and increases progressively  
419 from the bottom of the conduit to the surface. We solved the Navier-Stokes equations for  
420 an incompressible magma using this viscosity profile and applied the resulting stress at  
421 the conduit wall in order to calculate the displacement field. The other viscosity profile  
422 considered is obtained from *Collombet* [2009]. We used the stationary solution for flow  
423 conditions described by *Collombet* [2009] and applied the resulting stress at the conduit  
424 wall. In comparison with the previous models that only consider vertical gas escape, it  
425 also takes into account the lateral gas loss due to the permeability of the conduit wall.  
426 This model is suitable to model effusive activity, such as dome construction of andesitic  
427 strato-volcanoes because it allows to consider realistic initial volatiles content and to  
428 reproduce quite precisely the vesicularity of the degassed magma, which is consistent  
429 with the observations made on real domes. With this model, a large viscosity change  
430 occurs only in the upper few hundred metres of the conduit, which induces large stresses  
431 at the conduit wall close to the surface (Fig. 9a). The particularity of this last model is  
432 that, for shallow depths (above 750 m depth), magma overpressure in the conduit reaches  
433 larger values than those applied at the conduit bottom, due to magma compressibility  
434 effects. This large pressure gradient as well as the high shear stress at shallow levels of  
435 the conduit produced a tilt amplitude one order of magnitude larger than the two other  
436 models (Fig. 9b). Assuming a value of 0.8 GPa for the shear modulus and 10 MPa for  
437 the magma reservoir overpressure, the model obtained from *Collombet* [2009], taking into  
438 account a compressible magma and the vertical as well as the lateral degassing, seems

439 to better explain the amplitude of the tilt inflation measured in Soufrière Hills Volcano  
440 during the April-May period.

#### 4.4. Origin of Cyclic Deformation

441 The formation of a viscous plug in the shallow part reduces the magma flow rate and  
442 builds up large overpressures in the last few hundred metres, which may cause the tilt  
443 inflation observed at the surface. Plug formation is well explained by the magma viscosity  
444 increase as a consequence of exsolution, gas loss, cooling and crystallization processes. In  
445 order to account for the cyclic behaviour, an explanation for the following depressurisation  
446 is required. In most cases, the mechanism invoked is a stick-slip transition. Above a  
447 threshold criterion, rapid plug motion occurs because the magma starts to slip along the  
448 conduit walls, the speed of slip being a function of the wall friction. The plug is extruded  
449 and the magma pressure is released, causing the return to the initial state without the  
450 plug. The threshold criterion used is either a given overpressure within the magma below  
451 the plug [*Lensky et al.*, 2008] or the condition for brittle failure of the magma [*Collier and*  
452 *Neuberg*, 2006]. The onset of brittle failure has been identified to occur when the product  
453 of the melt viscosity and the shear strain rate is larger than the shear strength of the melt  
454 ( $\sigma_s$ ) [*Webb and Dingwell*, 1990], values being estimated between  $10^7$  and  $10^8$  Pa for pure  
455 glass [*Tuffen et al.*, 2003; *Tuffen and Dingwell*, 2005].

456 In our plug flow model, this criterion is equivalent to  $\tau_{up} = \frac{a_c P_p}{2 h_p} > \sigma_s$  and thus only  
457 depends on the conduit radius, the plug thickness and the pressure at the plug bottom.  
458 Largest shear stress is obtained for the most viscous and the thinnest plugs. From a value  
459 of magma shear strength of  $10^7$  Pa and classic values for Montserrat case of 15 m and  
460 10 MPa respectively for the conduit radius ( $a_c$ ) and the bottom pressure ( $P_c$ ), we deduce

461 than the plug length ( $h_p$ ) must be less than 7.5 m to reach the magma failure. *Burgisser*  
462 *et al.* [2011] suggest a thickness of a few tens of meters or even less for the dome plug,  
463 such that a thin plug might be possible. If we know consider a plug size of 50 m, a  
464 bottom overpressure larger than the 66.7 MPa is required for a 15 m radius conduit. In  
465 the case of a more realistic overpressure of 10 MPa, the brittle failure of the magma is  
466 obtained if the conduit radius is larger than 100 m. Based on these results, conditions  
467 required to cause magma failure remain unlikely, such that we used a no-slip condition  
468 at the conduit wall. However, there is some experimental as well as textural evidence  
469 of magma brittle failure in the upper portion of volcanic conduits [*Lavallée et al.*, 2008;  
470 *Tuffen et al.*, 2008]. The value of shear strength we used might be overestimated for real  
471 magma and our Newtonian flow model does not well describe the stress gradient close to  
472 the conduit where the deformation is expected to be very localised.

473 Another way to account for plug removal is to consider a modification of permeability at  
474 the conduit wall as proposed by *Edmonds et al.* [2003]. For example, *Taisne and Jaupart*  
475 [2008] have shown that the loading of the crater floor by the dome acts to prevent gas  
476 leakage from magma by closing fractures around the volcanic conduit. A permeability  
477 decrease would prevent lateral degassing and might reduce the plug either by decreasing  
478 its viscosity contrast or its length. This is consistent with the fact that, as at Soufrière  
479 Hills (Montserrat), a decrease in SO<sub>2</sub> emission rate was observed prior to the start of  
480 magma ascent, after a pause in dome growth [*Edmonds et al.*, 2003]. In this case, the  
481 evolution of the plug, from one state of equilibrium to another, requires more time than  
482 in the case of slip by rupture. Based on the flow rate and plug geometry, we can calculate  
483 the amount of time required for the entire extrusion of the plug. This value is represented

484 in Figure 7c and provides a lower bound for the duration of the deflation induced by the  
485 plug removal. In case of the calculation based on the viscosity profile taken from *Sparks*  
486 [1997], this duration is close to 12 hours whereas for the calculation based on the model  
487 developed by *Collombet* [2009] this duration is close to one hour, such that both models  
488 are consistent with the cycle duration recorded in 1997 at Montserrat Volcano.

#### 4.5. Origin of Tilt Reversals Before Eruptions

489 Reversals of ground tilt direction have been documented before eruptions. *Chadwick*  
490 *et al.* [1988] showed that before extrusions occurring at Mount St Helens from May 1981 to  
491 August 1982, outward tilting was observed during several weeks, accelerated sharply and  
492 then abruptly changed direction to inward tilting, minutes to hours before eruptive activity  
493 began. Such a phenomenon could be linked to a variation of magma pressure within a  
494 shallow reservoir. It would be consistent with a pressure increase due to replenishment or  
495 degassing occurring weeks before the eruptive event and followed by a pressure decrease as  
496 a response to magma discharge within a propagating dyke forming intrusion. However, in  
497 this case, the source of the ground deformation is likely to be located within the conduit as  
498 proposed by *Chadwick et al.* [1988]. A possible explanation might come from the evolution  
499 of the plug within the volcanic conduit. As shown in Figure 10, considering the plugged  
500 conduit as the reference state (high value of  $\frac{h_p}{L_c}$ ), the decrease of the plug thickness induces  
501 first an increase of the vertical displacement and tilt, correlated to a relative constant flow  
502 rate. These displacements correspond to a ground inflation with the slopes of the volcano  
503 tilting away from the volcanic vent. The inflation is followed by a decrease of ground  
504 displacements, which indicates a phase of rapid deflation. During this subsidence, the  
505 magma flow rate rapidly increases to reach its maximal value when the plug is totally

506 removed ( $\frac{h_p}{L_c} = 0$ ). Because the ground movement has changed in direction, the surface  
507 of the volcano now tilts towards the vent. As a result, the process of thickness variation  
508 development of a viscous plug in a volcanic conduit can be a possible origin for the tilt  
509 reversal observed before an eruption at andesitic volcanoes, such as Mount St Helens.

## 5. Conclusions

510 We estimated ground deformation induced at a volcano surface by magma viscosity  
511 changes occurring in the upper portion of the conduit. Calculations were performed  
512 considering a simplified viscosity profile for the magma, the viscosity taking two different  
513 values: a higher value within the plug and a lower value within the magma column  
514 itself, below. This model provides a good estimation of ground displacement, not very  
515 different, in amplitude, from the one produced by more realistic models with power-law  
516 profiles of viscosity. Plug emplacement results in a decrease of the magma discharge rate  
517 together with a rise of the shear stress levels along the conduit walls, which is considered  
518 to be the main source of displacements at the surface. However, even if it is most often  
519 dominant, the shear stress effect is not the only effect of importance: the conduit is also  
520 pressurized all along the conduit, the maximum of pressurization occurring at the plug  
521 bottom. This pressurization has a significant effect on surface deformation and should  
522 not be neglected. For the case of Soufrière Hills Volcano at Montserrat, neglecting the  
523 pressure effects leads to an overestimation, larger than 20 percent, of the tilt measured at  
524 500 m from the crater. Plug growth always results in an overall decreasing magma flow  
525 rate, whereas it may either induce an increase or a decrease of the outward tilt, depending  
526 on the magnitude and the depth of the pressurization level. Joint interpretation of magma

527 flow rates and surface displacements can bring strong constrain on the plug thickness and  
528 viscosity evolution. In absence of dome load or magma reservoir pressure variations, radial  
529 displacements or tilt signals caused by plug emplacement might be detected only a few  
530 hundred metres from the crater vent, according to the size and the viscosity of the plug  
531 as well as the size of the conduit and the mechanical properties of the host rocks. This  
532 conclusion becomes even more restrictive in case the dome geometry evolves by collapse  
533 or rapid magma emplacement or in case magma reservoir pressure variations occur. Then  
534 a plug emplacement might dominates the tilt as well as radial displacements only in the  
535 immediate vicinity of the conduit (less than 100 m). The estimated distance of detection  
536 should be taken into consideration when deciding for the type and the location of geodetic  
537 instrumentation at andesitic volcanoes. Or simplified model of plug emplacement can  
538 explain the amplitude around  $1 \mu rad$  of tilt signals recorded at Mt St Helens or Soufrière  
539 Hills Volcano at Montserrat in December 96. However, in order to explain the amplitude  
540 recorded, at Soufrière Hills, from May to August 2007, when the tilt reached more than 10  
541  $\mu rad$ , we need to consider compressible magma characterized by a more realistic viscosity  
542 profile resulting from vertical as well as lateral degassing.

## Appendix A: Fluid-Solid Interaction

In our study, we treat the full coupling between the fluid and the elastic solid by an iterative process. At each step, we solve for the fluid flow, apply the resulting stress components at the conduit wall, and then we calculate the displacements at the conduit walls and modify, in consequence, the geometry of the fluid domain boundaries. We iterate this process chain until convergence occurs. Usually convergence is immediate because the radial displacements of the conduit wall is small. This radial displacement can be

approximated analytically. Neglecting the tangential stress effects and considering that the pressure gradient with depth remains small, we can use the solution of an infinite pressurised pipe with an axial geometry to estimate, to a first approximation, the radial displacement of the conduit wall. It gives  $U_r = \frac{1}{2} \left( \frac{P_c}{G} \right) a_c$  [Landau and Lifshitz, 1975; Love, 1987], where  $P_c$  is the overpressure at the conduit bottom,  $G$  the shear modulus of host rocks and  $a_c$  the conduit radius. In volcanic conduits, the magma overpressure does not exceed values of 20 MPa [Melnik and Sparks, 1999] and the shear modulus is around 1-10 GPa [Costa et al., 2007b; Voight et al., 1999; Barmin et al., 2002]. So, the amplitude, therefore, of the radial displacement ( $U_r$ ) at the conduit wall remains smaller than 1% of the conduit radius. For a 10 metre radius, the expected maximal wall displacement will be only 10 centimeters. We quantified, in our plug model, the effect of this wall deformation on the displacement field at the surface. First, wall deformation has a larger effect for a low shear modulus ( $G$ ) and a large overpressure ( $P_c$ ). Secondly, from a shear modulus of 0.4 GPa and a magma overpressure of 10 MPa, the amplitude of the surface displacements is only 5% larger when we take into account the conduit wall deformation compared with the rigid conduit case. In many volcanic contexts, the effect of conduit wall deformation will not affect significantly the surface displacements and can thus be neglected to a first approximation.

## Appendix B: Model validation

Numerical solutions have been compared to existing analytic solutions in order to validate our model. First we used our numerical simulation to estimate the radial displacement induced, at the surface, by a pressurized pipe, with a uniform pressure  $P_c$ , embedded in an elastic half-space. Results were compared with the solution given by the following

analytic expression [Love, 1987]:  $U_r = \frac{a_c^2 P_c}{2rG}$ , where  $r$  is the radial distance. Secondly, the tilt induced, at the surface, by a constant shear stress applied along the conduit wall, was numerically estimated and compared to the analytic expression provided by *Anderson et al.* [2010], which corresponds to an approximate solution derived from the integration of the Green's functions of a vertical point force. The comparison between numerical results and analytic solutions as well as the estimated error are shown in Figure 11. The error is the relative difference in percent between the analytic calculation and our numerical results. This figure shows that the error is the largest at the smallest distance from the conduit. However, for a distance larger than 50 meters, the error remains smaller than 2 % for the pressurised pipe (case a) and close to 0 for the conduit with an applied shear stress (case b).

**Acknowledgments.** This study was supported by IRD. We are very grateful for helpful reviews from the Associate Editor M. Ryan, A. Costa, V. Cayol and an anonymous reviewer.

## References

- Anderson, K., M. Lisowski, and P. Segall, Cyclic ground tilt associated with the 2004-2008 eruption of mount St. Helens, *J. Geophys. Res.*, *115*, 2010.
- Barmin, A., O. Melnik, and R. Sparks, Periodic behavior in lava dome eruptions, *Earth Planet. Sci. Lett.*, *199*, 173–184, 2002.
- Beauducel, F., F.-H. Cornet, E. Suhanto, T. Duquesnoy, and M. Kasser, Constraints on magma flux from displacements data at Merapi volcano, Java, Indonesia, *J. Geophys. Res.*, *105*, 8193–8203, 2000.

- Bonaccorso, A., and P. Davis, Models of ground deformation from vertical conduits with application to eruptions of Mount St. Helens and Mount Etna, *J. Geophys. Res.*, *104*, 10,531–10,542, 1999.
- Burgisser, A., S. Poussineau, L. Arbaret, T. Druitt, T. Giachetti, and J.-L. Bourdier, Pre-explosive conduit conditions of the 1997 Vulcanian explosions at Soufrière Hills Volcano, Montserrat: I. Pressure and vesicularity distributions, *J. Volcanol. Geotherm. Res.*, *194*, 27–41, 2010.
- Burgisser, A., L. Arbaret, T. Druitt, and T. Giachetti, Pre-explosive conduit conditions of the 1997 Vulcanian explosions at Soufrière Hills Volcano, Montserrat: II. Overpressure and depth distributions, *J. Volcanol. Geotherm. Res.*, *199*, 193–205, 2011.
- Caricchi, L., L. Burlini, P. Ulmer, T. Gerya, M. Vassalli, and P. Papale, Non-Newtonian rheology of crystal-bearing magmas and implications for magma ascent dynamics, *Earth Planet. Sci. Lett.*, *264*, 402–419, 2007.
- Cayol, V., and F. Cornet, Effects of topography on the interpretation of the deformation field of prominent volcanoes - Application to Etna, *Geophys. Res. Letters*, *25*, 1979–1982, 1998.
- Chadwick, W., R. Archuleta, and D. Swanson, The Mechanics of Ground Deformation Precursory to Dome-Building Extrusions at Mount St. Helens 1981-1982, *J. Geophys. Res.*, *93*, 4351–4366, 1988.
- Collier, L., and J. Neuberg, Incorporating seismic observations into 2D conduit flow modeling, *J. Volcanol. Geotherm. Res.*, *152*, 331–346, 2006.
- Collombet, M., Two-dimensional gas loss for silicic magma flows: toward more realistic numerical models, *Geophys. J. Int.*, *177*, 309–318, 2009.

- Costa, A., and G. Macedonio, Viscous heating in fluids with temperature-dependent viscosity: Triggering of secondary flows, *J. Fluid Mech.*, *540*, 21–38, 2005.
- Costa, A., O. Melnik, and R. Sparks, Controls of conduit geometry and wallrock elasticity on lava dome eruptions, *EPSL*, *260*, 137–151, 2007a.
- Costa, A., O. Melnik, R. Sparks, and B. Voight, Control of magma flow in dykes on cyclic lava dome extrusion, *Geophys. Res. Letters*, *34*, L02,303, 2007b.
- Costa, A., O. Melnik, and E. Vedeneeva, Thermal effects during magma ascent in conduits, *J. Geophys. Res.*, *112*, 2007c.
- Denlinger, R., and R. Hoblitt, Cyclic eruptive behavior of silicic volcanoes, *Geology*, *27*, 459–462, 1999.
- Edmonds, M., C. Oppenheimer, D. Pyle, R. Herd, and G. Thompson, SO<sub>2</sub> emissions from Soufrière Hills Volcano and their relationship to conduit permeability, hydrothermal interaction and degassing regime, *J. Volcanol. Geotherm. Res.*, *124*, 23–43, 2003.
- Gardner, J., R. Thomas, C. Jaupart, and S. Tait, Fragmentation of magma during Plinian volcanic eruptions, *Bull. Volcanol.*, *58*, 144–162, 1996.
- Green, D., J. Neuberg, and V. Cayol, Shear stress along the conduit wall as a plausible source of tilt at Soufrière Hills volcano, Montserrat, *Geophys. Res. Letters*, *33*, L10,306, 2006.
- Harris, A., W. Rose, and L. Flynn, Temporal trends in lava dome extrusion at Santiaguito 1922–2000, *65*, 77–89, 2002.
- Hautmann, S., J. Gottsmann, R. Sparks, A. Costa, O. Melnik, and B. Voight, Modelling ground deformation caused by oscillating overpressure in a dyke conduit at Soufrière Hills Volcano, Montserrat, *Tectonophysics*, *471*, 87–95, 2009.

- Hess, K.-U., and D. Dingwell, Viscosities of hydrous leucogranitic melts: A non-Arrhenian model, *American Mineralogist*, *81*, 1297–1300, 1996.
- Iverson, R., et al., Dynamics of seismogenic volcanic extrusion at Mount St Helens in 2004-05, *Nature*, *444*, 439–443, 2006.
- Landau, L., and E. Lifshitz, *Theory of elasticity*, 2nd ed. ed., Pergamon, Tarrytown, N.Y., 1975.
- Lavallée, Y., P. Meredith, D. Dingwell, K.-U. Hess, J. Wassermann, B. Cordonnier, A. Gerik, and J. Kruhl, Seismogenic lavas and explosive eruption forecasting, *Nature*, *453*, 507–509, 2008.
- Lejeune, A., and P. Richet, Rheology of crystal-bearing silicate melts: An experimental study at high viscosities, *J. Geophys. Res.*, *100*, 4215–4229, 1995.
- Lensky, N., R. Sparks, O. Navon, and V. Lyakhovsky, Cyclic activity at Soufrière Hills Volcano, Montserrat: degassing-induced pressurization and stick-slip extrusion, in *Fluid Motions in Volcanic Conduits: A Source of Seismic and Acoustic Signals*, vol. 307, Geological Society ed., pp. 169–188, Lane, S.J. & Gilbert, J.S., London, 2008.
- Lister, J., and R. Kerr, Fluid-Mechanical models of crack propagation and their application to magma transport in dikes, *J. Geophys. Res.*, *96*, 10,049–10,077, 1991, archimede.
- Llewellyn, E., and M. Manga, Bubble suspension rheology and implications for conduit flow, *J. Volcanol. Geotherm. Res.*, *143*, 205–217, 2005.
- Love, A., *A Treatise on the mathematical theory of elasticity*, Dover Classics of Sciences and Mathematics, 4th ed., Dover, 1987.
- Mastin, G., and D. Pollard, Surface Deformation and Shallow Dike Intrusion Processes at Inyo Craters, Long Valley, California, *J. Geophys. Res.*, *93*, 13,221–13,235, 1988.

- Melnik, O., and R. Sparks, Nonlinear dynamics of lava dome extrusion, *Nature*, *402*, 37–41, 1999.
- Melnik, O., and R. Sparks, Controls on conduit magma flow dynamics during lava dome building eruptions, *J. Geophys. Res.*, *110*, 2005.
- Mogi, K., Relations between the eruptions of various volcanoes and the deformation of the ground surfaces around them, *Bull. Earthquake Res. Inst., Univ. Tokyo*, *36*, 99–134, 1958, analytic.
- Nakada, S., and J. Eichelberger, Looking into a volcano: drilling Unzen, *Geotimes*, *49*, 14–17, 2004.
- Nakada, S., H. Shimizu, and K. Ohta, Overview of the 1990-1995 eruption at Unzen Volcano, *J. Volcanol. Geotherm. Res.*, *89*, 1–22, 1999.
- Nishimura, T., Ground deformation due to magma ascent with and without degassing, *Geophys. Res. Letters*, *33*, L23,309, 2006.
- Nishimura, T., Ground deformation caused by magma ascent in an open conduit, *J. Volcanol. Geotherm. Res.*, *187*, 178–192, 2009.
- Pinkerton, H., and R. Stevenson, Methods of determining the rheological properties of magmas at sub-liquidus temperatures, *J. Volcanol. Geotherm. Res.*, *53*, 47–66, 1992.
- Roman, D., J. Neuberg, and R. Luckett, Assessing the likelihood of volcanic eruption through analysis of volcanotectonic earthquake fault-plane solutions, *Earth Planet. Sci. Lett.*, *248*, 244–252, 2006.
- Rubin, A., Propagation of magma-filled cracks, *Ann. Rev. Earth Planet. Sci.*, *23*, 287–336, 1995.

- Shaw, H., Obsidian-H<sub>2</sub>O Viscosities at 1000 and 2000 Bars in the Temperature Range 700° to 900°C, *J. Geophys. Res.*, *68*, 6337–6343, 1963.
- Sparks, R., Causes and consequences of pressurisation in lava dome eruptions, *Earth Planet. Sci. Lett.*, *150*, 177–189, 1997.
- Sparks, R., and S. Young, The eruption of Soufrière Hills volcano, Montserrat (1995-1999): overview of scientific results, in *The eruption of the Soufrière Hills Volcano, Montserrat from 1995 to 1999*, edited by T. Druitt and B. Kokelaar, pp. 45–69, Geological Society, 2002.
- Sparks, R., M. Murphy, A. Lejeune, R. Watts, J. Barclay, and S. Young, Control on the emplacement of the andesite lava dome of the Soufrière Hills Volcano, Montserrat by degassing-induced crystallization, *Terra Nova*, *12*, 14–20, 2000.
- Swanson, D., and R. Holcomb, Regularities in growth of the Mount St. Helens dacite dome 1980-1986, in *Lava Flows and Domes: Emplacement and Mechanisms and Hazards Implications*, Springer ed., pp. 3–24, J.H. Fink, New York, 1990.
- Taisne, B., and C. Jaupart, Magma Degassing and Intermittent Lava Dome Growth, *Geophys. Res. Letters*, *35*, 2008.
- Tuffen, H., and D. Dingwell, Fault textures in volcanic conduits: evidence for seismic trigger mechanisms during silicic eruptions, *Bull. Volcanol.*, *67*, 370–387, 2005.
- Tuffen, H., D. Dingwell, and H. Pinkerton, Repeated fracture and healing of silicic magma generate flow banding and earthquakes?, *Geology*, *31*, 1089–1092, 2003.
- Tuffen, H., R. Smith, and R. Sammonds, Evidence for seismogenic fracture of silicic magma, *Nature*, *453*, 511–513, 2008.

- Voight, B., R. Hoblitt, A. Clarke, A. Lockhart, A. Miller, L. Lynch, and J. McMahon, Remarkable cyclic ground deformation monitored in real-time on Montserrat, and its use in eruption forecasting, *Geophys. Res. Letters*, *25*, 3405–3408, 1998.
- Voight, B., E. Constantine, S. Siswamidjono, and R. Torley, Historical eruptions of Merapi Volcano, central Java, Indonesia, 1768-1998, *J. Volcanol. Geotherm. Res.*, *100*, 69–138, 2000.
- Voight, B., et al., Magma Flow Instability and Cyclic Activity at Soufriere Hills Volcano, Montserrat, British West Indies, *Science*, *283*, 1999.
- Voight, B., et al., Unprecedented pressure increase in deep magma reservoir triggered by lava-dome collapse, *Geophys. Res. Letters*, *33*, 2006.
- Watson, I., et al., The relationship between degassing and ground deformation at Soufriere Hills Volcano, Montserrat, *J. Volcanol. Geotherm. Res.*, *98*, 117–126, 2000.
- Webb, S., and D. Dingwell, Non-Newtonian Rheology of Igneous Melts at High Stresses and Strain Rates: Experimental Results for Rhyolite, Andesite, Basalt, and Nephelinite, *J. Geophys. Res.*, *95*, 15,695–15,701, 1990.
- Williams, P., and S. Self, The October 1902 Plinian eruption of Santa Maria volcano, Guatemala, *J. Volcanol. Geotherm. Res.*, *16*, 1983.
- Wylie, J., B. Voight, and J. Whitehead, Instability of Magma Flow from Volatile-Dependent Viscosity, *Science*, *285*, 1999.
- Yokoyama, I., Geophysical characteristics of dacite volcanism 1977-1978 eruption of Usu volcano, *J. Volcanol. Geotherm. Res.*, *9*, 335–358, 1981.

**Figure 1.** a) Schematic representation of the plugged conduit model. Geometric and physical parameters are shown. No displacement in the direction perpendicular to the surface is allowed at the right and lower boundaries. The upper boundary is a free surface. The right boundary is situated far away from the conduit (at 100 km) in order to prevent boundary effects. Fluid flow is caused by pressure difference between the conduit bottom ( $P = P_c$ ) and the surface ( $P = 0$ ). A no-slip condition is applied at the fluid along the conduit wall. The continuity of the stress field, normal as well as tangential components, is applied at the conduit wall. The formation of the plug at the top of the conduit is modelled by an increase of the magma viscosity. b) 1-D viscosity profile used in our calculation (left side) and the resulting stresses (pressure and shear stress) at the conduit wall (right side). As a first approximation, the increase of the viscosity is modelled by a "step" function, with two extreme values: the viscosity in the magma column below the plug,  $\mu_m$ , and the viscosity of the plug,  $\mu_p$ . We consider an incompressible magma with constant density. In each sketch, dashed curves represented our reference case: the Poiseuille flow with a constant viscosity ( $\mu = \mu_m$  at any depth).

**Figure 2.**

a) Mesh of the numerical model superimposed to the pattern of total displacements induced within the host rocks by a Poiseuille magma flow. The mesh is highly refined in the region close to the conduit, where the gradient of displacements are the largest. Displacements are induced by a flow at constant viscosity initiated by a pressure of 10 MPa at the bottom of a conduit. The conduit is a cylinder with a 15 m radius and a 5000 m length. Elastic parameters of the host rocks are respectively 4 GPa and 0.25 for the shear modulus  $G$  and the Poisson's ratio  $\nu$ . Note that in lateral extension only the first 10 km of the 100 km corresponding to the actual box size, are shown. b) Zoom of the mesh in the 1 km<sup>2</sup> area near the surface corresponding to the red box of Figure a).

**Figure 3.** Surface displacements: radial (a), vertical (b) and tilt (c) induced by a constant viscosity magma flow (reference case chosen in the following). Displacements are obtained with respect to the lithostatic medium containing an overpressurized reservoir not connected to the surface with a Poisson's ratio equal to 0.25. Results are presented for three different conduit aspect ratio ( $\frac{a_c}{L_c}$ ). Distances are normalized by the conduit length ( $L_c$ ) and displacement by the ratio ( $\frac{P_c}{G}L_c$ ). The distance  $r=0$  corresponds to the conduit wall. In each case, the total displacement (solid line) as well as displacement only induced by the shear stress component (short dashed) or by the pressure (large dashed) are shown.

**Figure 4.** Tilt induced by the formation of a plug at the top of the conduit, shown as a function of the two dimensionless numbers characterizing the plug: the length ratio ( $\frac{h_p}{L_c}$ ) and the viscosity ratio ( $\frac{\mu_p}{\mu_m}$ ). Tilt is calculated, at the surface, 500 m away from the conduit wall. Results are shown for a given conduit geometry, with a radius ( $a_c$ ) of 15 m and a length ( $L_c$ ) of 5000 m. The pressure  $P_c$  applied at the bottom is fixed at 10 MPa, the shear modulus of the host rocks,  $G$ , is equal to 0.8 GPa and the Poisson's ratio is set to 0.25. a) Part of the tilt which is only induced by the shear stress applied at the conduit wall. b) Part of the tilt which is only induced by the pressure applied at the conduit wall. Tilt represented in c) is the summation of the values shown in b) and c). The dashed line corresponds to the critical plug thickness,  $h_{p(crit)}$ , which gives the maximal tilt value for a given viscosity ratio. Note that tilt is relative to our reference case obtained with a constant viscosity magma flow, which means that tilt tends to zero when either  $h_p$  tends to zero or the viscosity ratio  $\frac{\mu_p}{\mu_m}$  tends to 1.

**Figure 5.** Detection distance for the horizontal (a) and vertical (b) displacements as a function of the two dimensionless numbers related to the plug: the length ratio ( $\frac{h_p}{L_c}$ ) and the viscosity ratio ( $\frac{\mu_p}{\mu_m}$ ). The detection distance here corresponds to the maximal radial distance from the conduit wall where, respectively, a horizontal and a vertical displacement larger in amplitude than, respectively, one mm and 1 cm, is expected. The conduit length ( $L_c$ ) and the pressure ( $P_c$ ) applied at the bottom are, respectively, set to 5000 m and 10 MPa. The Poisson's ratio is set to 0.25 and  $a_c = 15$  m and  $G = 0.8$  GPa.

**Figure 6.** Detection distance for the tilt signal, function of the two dimensionless numbers related to the plug: the length ratio ( $\frac{h_p}{L_c}$ ) and the viscosity ratio ( $\frac{\mu_p}{\mu_m}$ ). The detection distance here corresponds to the maximal radial distance from the conduit wall where a tilt larger in amplitude than one microradian is expected. The conduit length ( $L_c$ ) and the pressure ( $P_c$ ) applied at the bottom are, respectively, set to 5000 m and 10 MPa. The Poisson's ratio is set to 0.25. Results are presented for four different cases: a)  $a_c = 50$  m and  $G = 0.8$  GPa b)  $a_c = 50$  m and  $G = 4.0$  GPa, c)  $a_c = 15$  m and  $G = 0.8$  GPa and d)  $a_c = 15$  m and  $G = 4.0$  GPa.

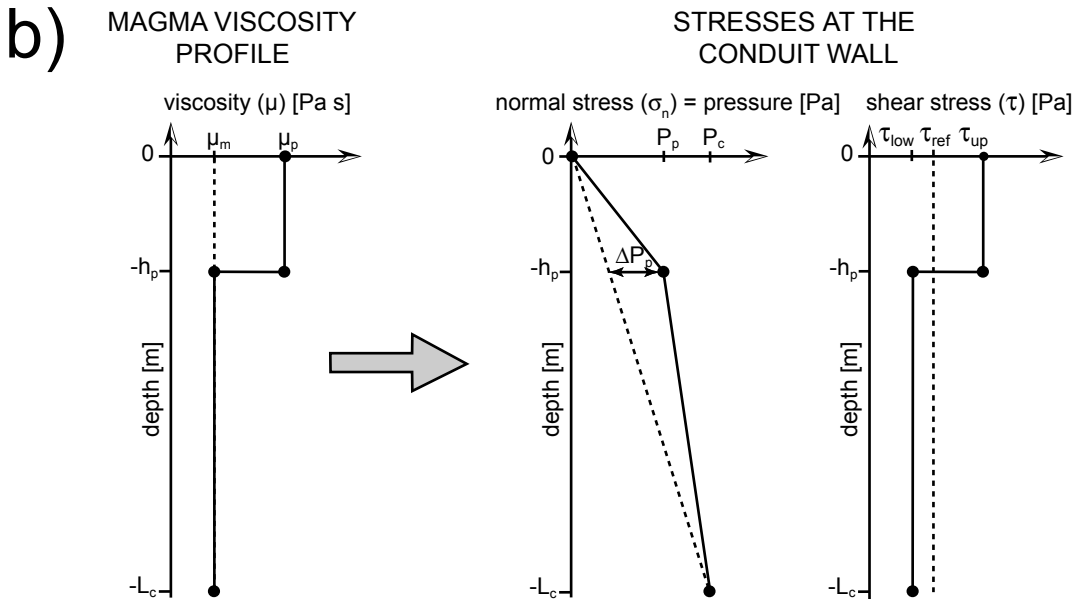
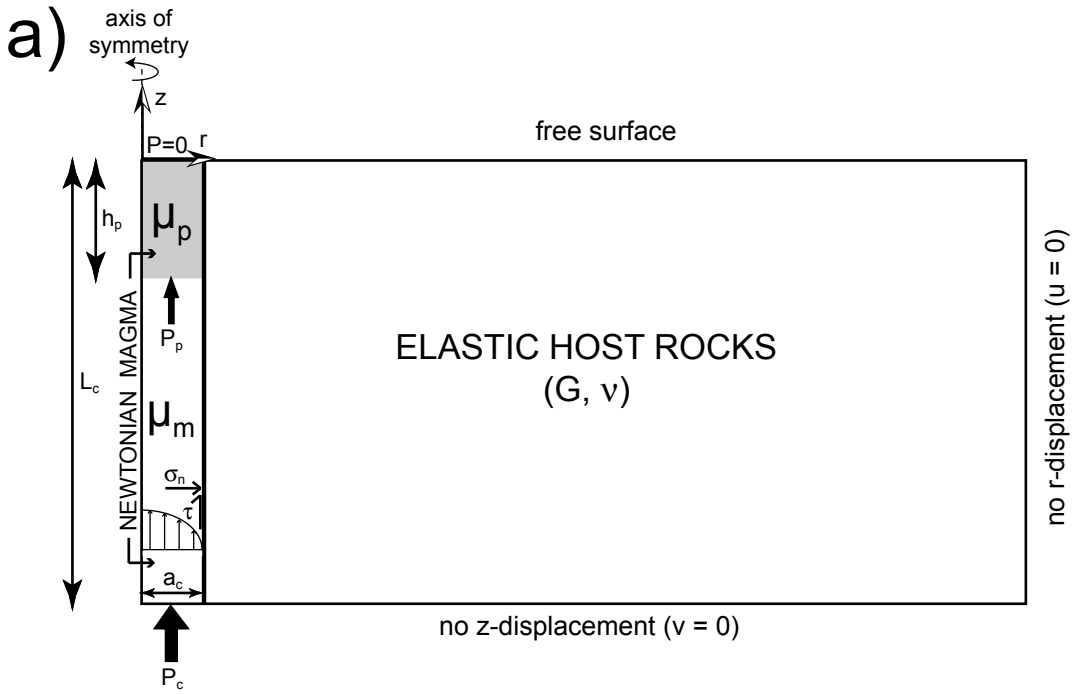
**Figure 7.** Relationship between tilt signal, magma flow rate and extrusion duration during the evolution of a plug within the volcanic conduit. Conditions are, as for Figure 4, obtained for a conduit radius ( $a_c$ ) of 15 m, a conduit length ( $L_c$ ) of 5000 m, a bottom pressure ( $P_c$ ) of 10 MPa, a shear modulus ( $G$ ) equal to 0.8 GPa and a Poisson's ratio ( $\nu$ ) set to 0.25. Two end-members for the plug evolution are tested: (1) a viscosity increase of plugs having a given thickness (left panels) ; (2) a thickness increase for plugs having a constant viscosity (right panels). For each case, we show a) Tilt calculated at a radial distance of 500 m from the conduit ; b) Normalized magma flow rate ( $Q/Q_{ref}$ ) deduce from the expression (3) ; c) Extrusion duration in hours, which corresponds to the amount of time required to totally extrude the plug considered (with thickness  $h_p$  and viscosity  $\mu_p$ ). This parameter is directly inferred from the ratio between the volume of the plug ( $\pi a_c^2 h_p$ ) and the magma flux  $Q$ , when the value of the magma viscosity  $\mu_m$  is set. Here, the extrusion duration is obtained taking  $\mu_m = 10^4$  Pa.s.

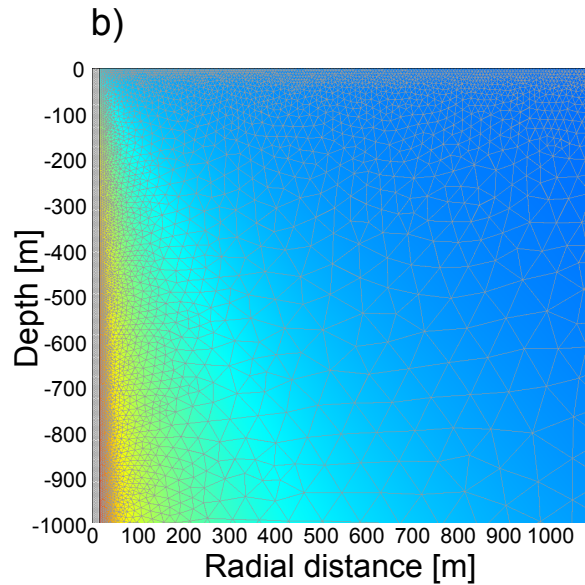
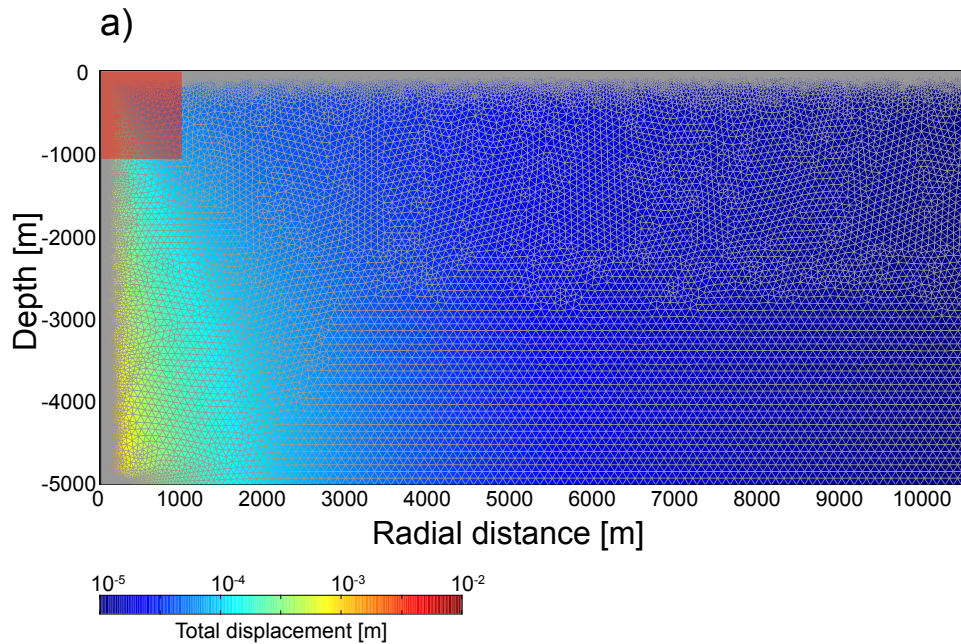
**Figure 8.** Amplitude of surface ground motion : a) the radial and b) vertical displacements as well as c) the tilt for various processes occurring on andesitic strato-volcanoes, detailed on sketch d). Numerical calculations are performed with the COMSOL software, taking a value of 0.8 GPa for rocks rigidity and 0.25 for the Poisson's ratio. The reference state is an overpressurized reservoir ( $P_c = \rho_m g L_c + 10$  MPa) embedded in a lithostatic medium, which feeds an open conduit with length ( $L_c$ ) and radius ( $a_c$ ) respectively equal to 5000 m and 15 m. Magma in the conduit has a constant viscosity ( $\mu_m$ ). Perturbations are the following: (1) Overpressure change of  $\Delta P_c = 1$  MPa due to magma replenishment or withdrawal within a  $10 \text{ km}^3$  spherical magma reservoir (long dashed curves in a-b-c). (2) Plug emplacement in the upper part of the conduit, characterised by a thickness ( $h_p$ ) of 50 m and a viscosity ratio ( $\frac{\mu_p}{\mu_m}$ ) equal to  $10^5$  (solid curves in a-b-c). (3) Load change of  $P_d = 1$  MPa due to the construction/destruction of a 200 m radius ( $R_d$ ) lava dome at the surface (short dashed curves in a-b-c). Note that the value of 1 MPa can be associated to a dome height variation of 60 m for eruptive products density of  $1700 \text{ kg.m}^{-3}$ .

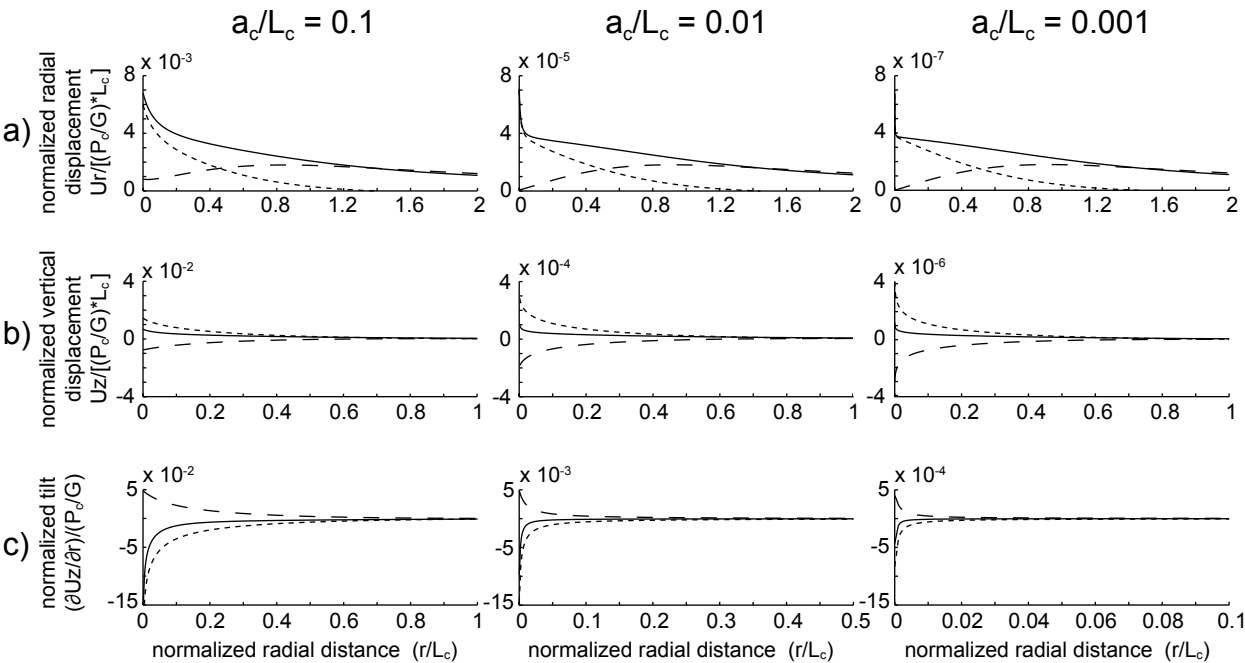
**Figure 9.** a) Magma viscosity as a function of normalized depth (left side) and resulting stress components along the conduit wall (right side) for various models. Note that stress components represented are the differential terms compared to the lithostatic stress field. Black lines correspond to plug models described in our study. Four models are tested with the same viscosity contrast ( $\frac{\mu_p}{\mu_m} = 10^5$ ) but different length ratio:  $\frac{h_p}{L_c} = 0.01$ ,  $\frac{h_p}{L_c} = 0.05$ ,  $\frac{h_p}{L_c} = 0.10$  and  $\frac{h_p}{L_c} = 0.25$ . Red and blue lines correspond to calculation with more realistic profile for magma viscosity, which depends on the gas escape process occurring on the magma column. The first (red) is derived from *Sparks* [1997], where depth dependence of magma viscosity is expressed as a power-law function. The second (blue), deduced from the study of *Collombet* [2009], considers vertical gas loss as the previous, but also the lateral gas escape due to wall permeability. b) Tilt signal at the surface induced by the different flow models discussed in a). The reference state is the Poiseuille flow with a constant viscosity. The blue boxes indicate the tilt amplitude recorded in two andesitic volcanoes: (1) and (2) at Soufrière Hills (Montserrat) respectively in May-August 1997 and December 1996 [*Voight et al.*, 1998] ; (3) at Mt St Helens between July 2006 and January 2007 [*Anderson et al.*, 2010]. Parameters used for the calculation are the same as in Figure 4.

**Figure 10.** a) Evolution of the tilt calculated at 500 m from the conduit (black line) and the magma flow rate (grey line) during the plug thickness decrease. The viscosity ratio  $\frac{\mu_p}{\mu_m}$  is fixed at 100. All parameters are the same as in Figure 7. The dots associated with numbers correspond to different cases of plug thickness, from 1 (very thick) to 4 (very thin). The last case, number 5, is related to a model without plug. b) Sketch showing the evolution of ground movement and magma flow rate during the decrease of a plug thickness. From case 3 to 4, we see a change in the direction of ground movement (inflation to subsidence) correlated with a strong increase of the magma flux. Both changes could be used as precursors in the eruption forecasting of andesitic volcanoes.

**Figure 11.** Analytic (solid lines) against numerical solutions (dots) for ground surface motion: a) the radial displacements induced by a pressurized conduit and b) the tilt induced by a vertical traction along the conduit wall. The conduit is a cylinder with a 15 m radius and a 5000 m length. Elastic medium is characterized by a shear modulus of 0.8 GPa and a Poisson's ratio of 0.25. In a), all the conduit is pressurized with a uniform pressure equal to 10 MPa. In b), the shear stress equal to 3000 Pa is applied in the lower part of the conduit, between -2500 and -5000 m depth. The bottom panels show for each case the relative difference in percent between analytic and numerical solutions.

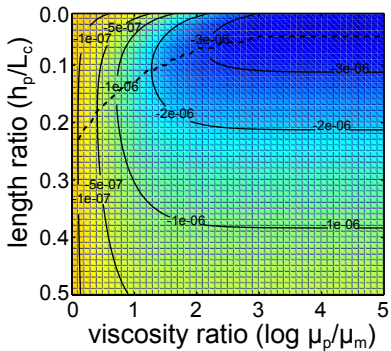




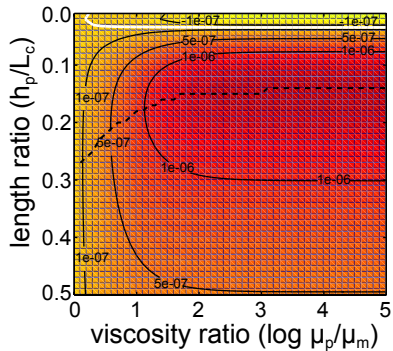


- shear stress
- - - - - pressure
- shear stress + pressure

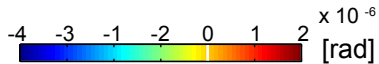
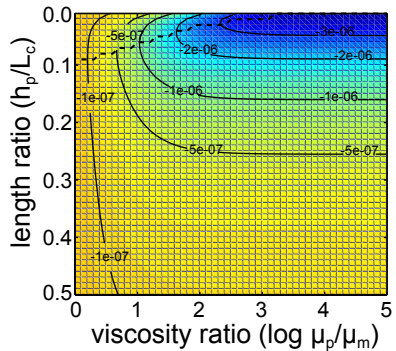
a) Shear stress

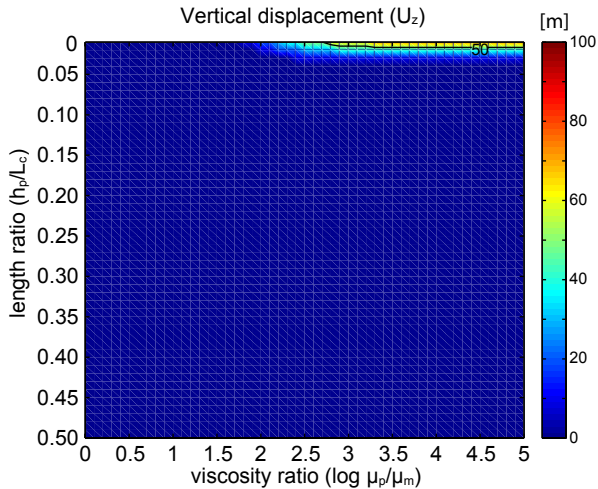
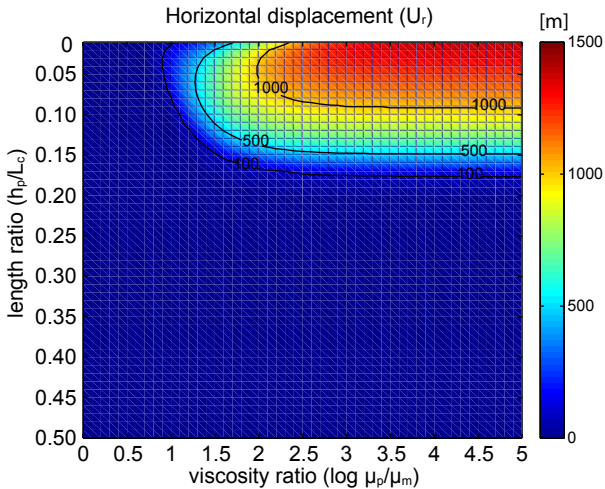


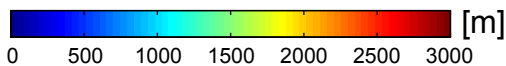
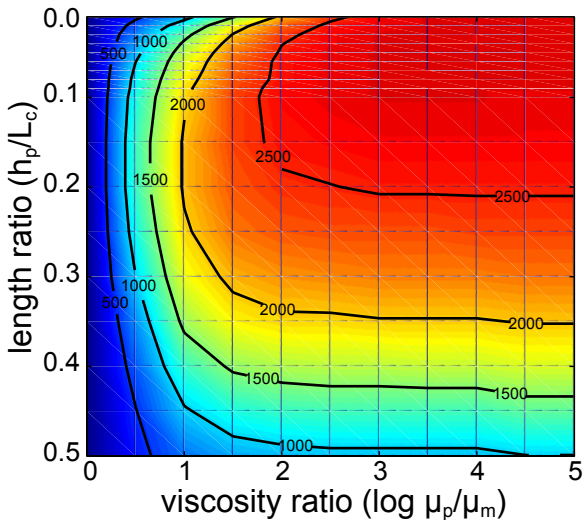
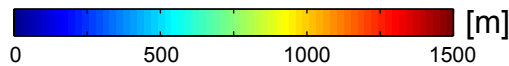
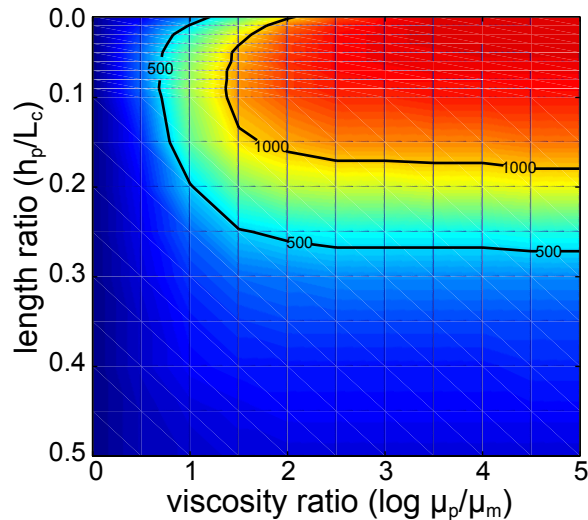
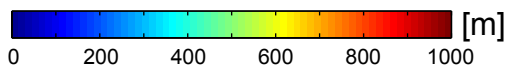
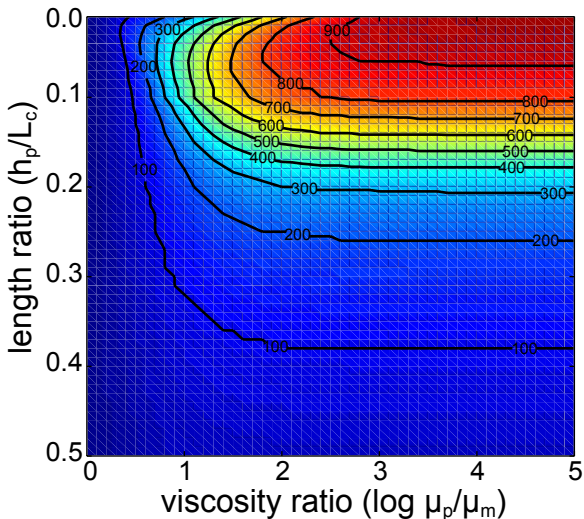
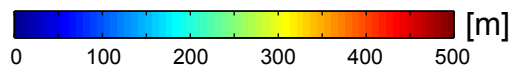
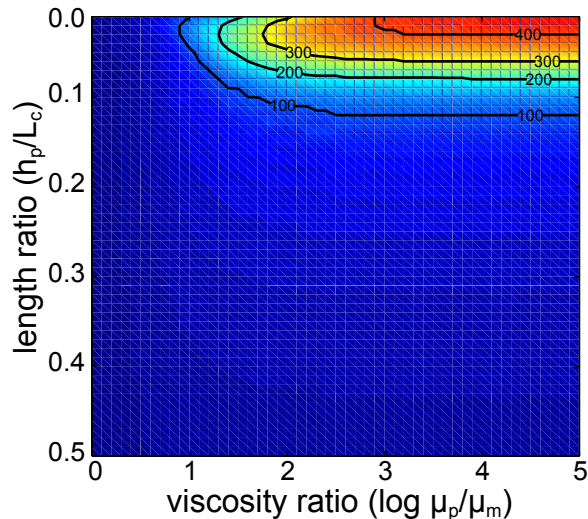
b) Pressure



c) Shear + pressure

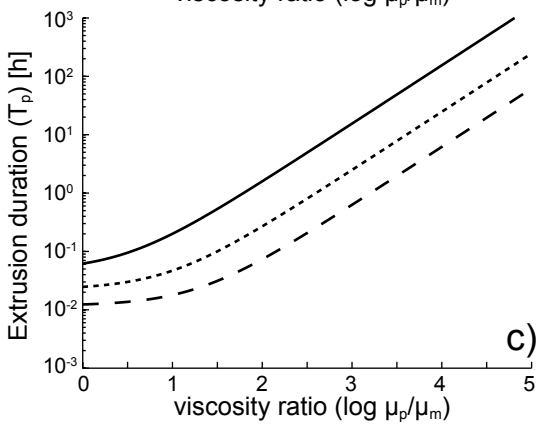
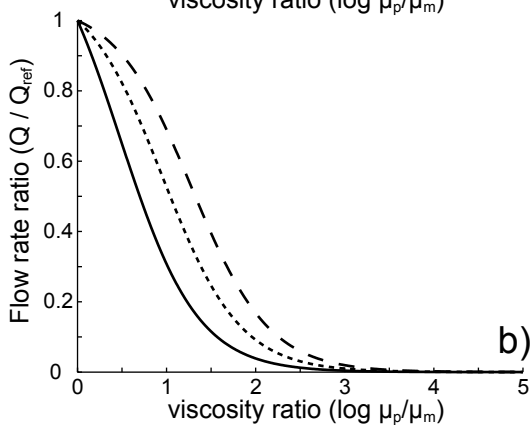
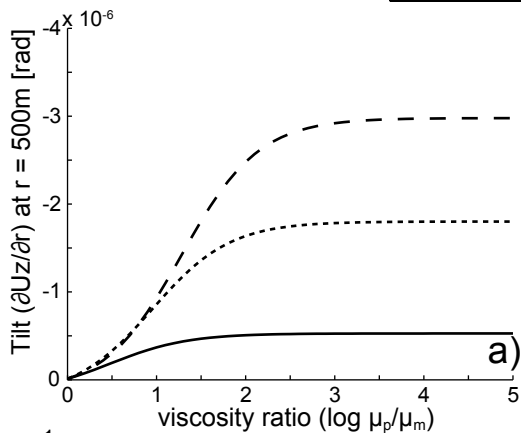
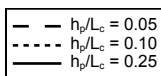




a)  $a_c = 50$  m -  $G = 0.8$  GPab)  $a_c = 50$  m -  $G = 4$  GPac)  $a_c = 15$  m -  $G = 0.8$  GPad)  $a_c = 15$  m -  $G = 4$  GPa

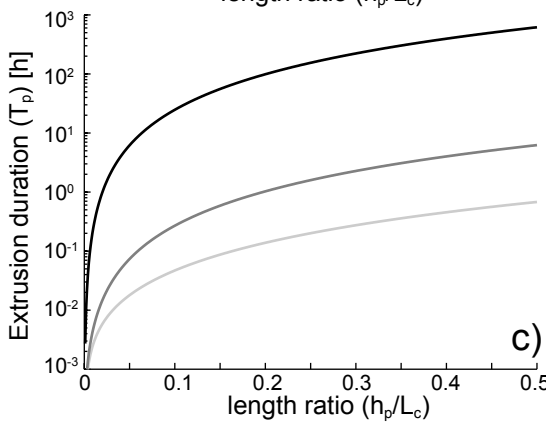
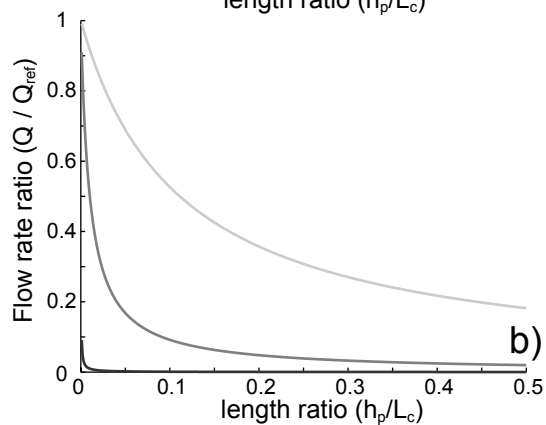
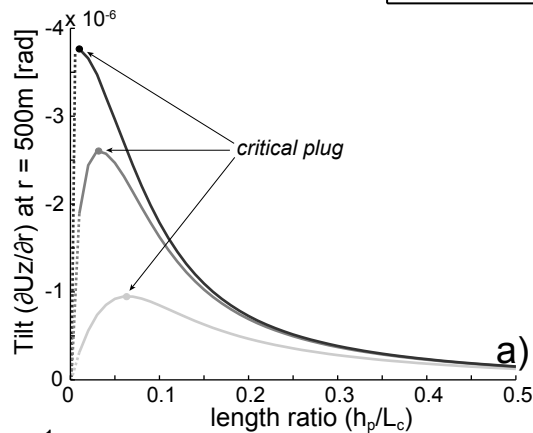
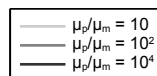
# (1) Plug viscosity

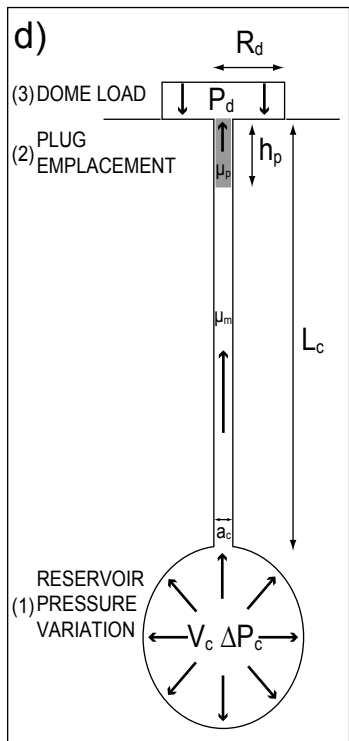
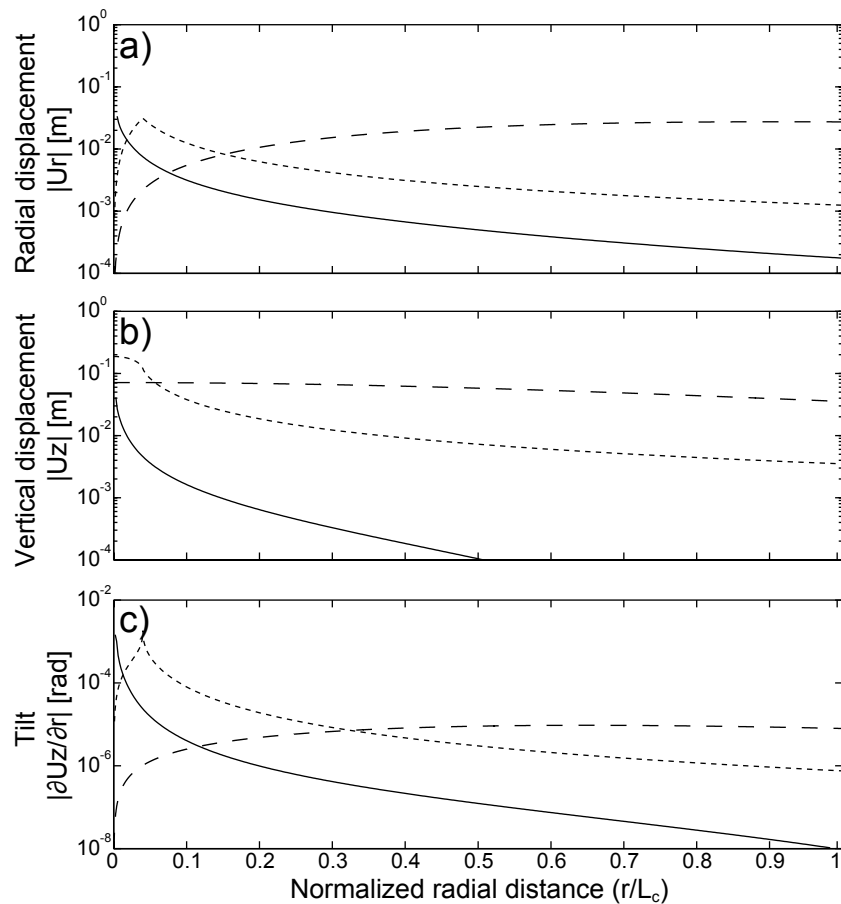
increase



# (2) Plug thickness

increase

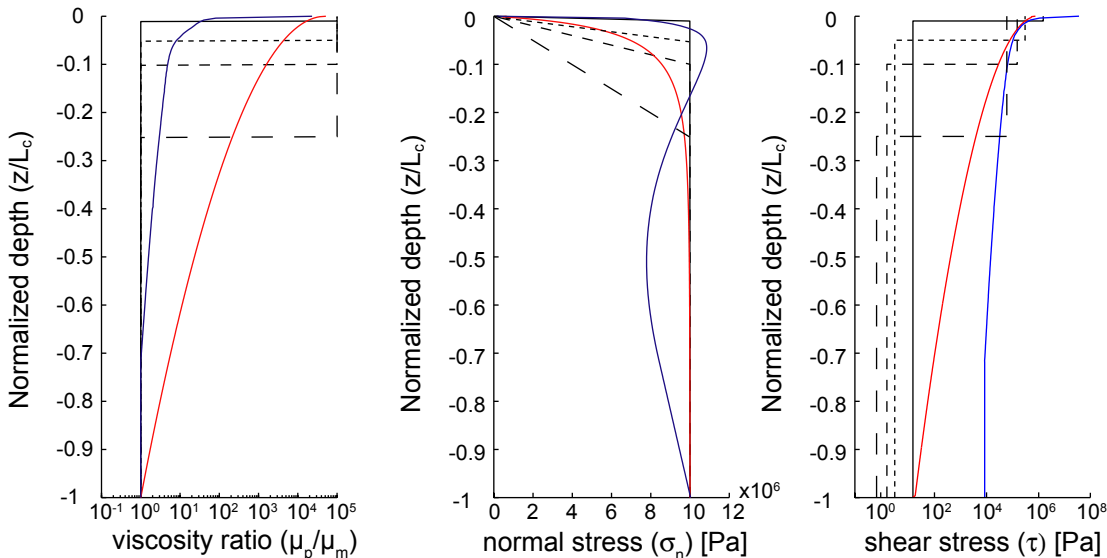




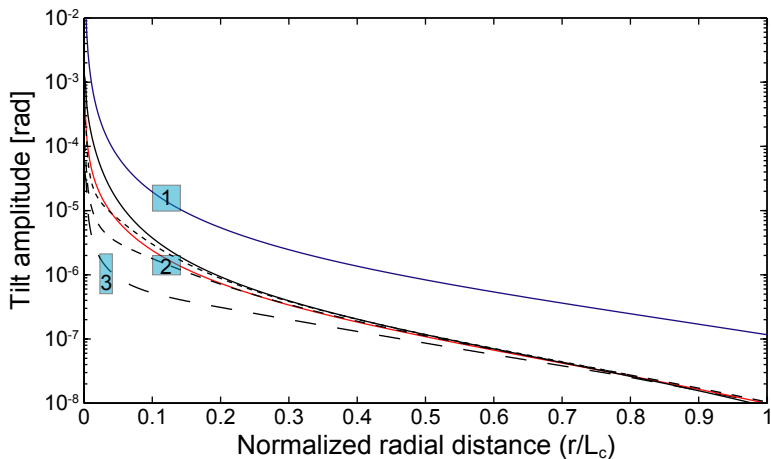
### Legend

- reservoir pressure (1)
- conduit flow (2)
- ..... dome load (3)

# a) Depth profile of the viscosity and the resulting stresses at the conduit wall



# b) Tilt at the surface



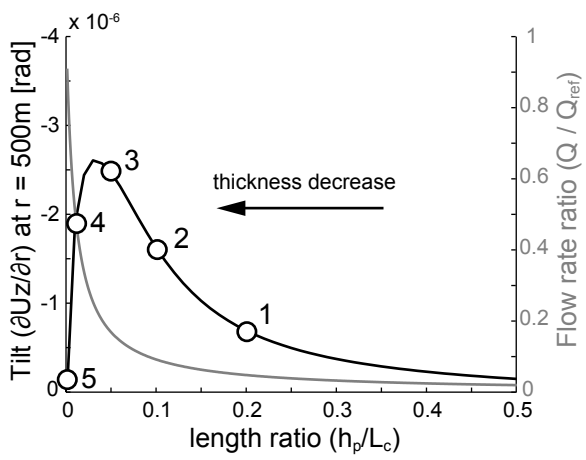
## Our plug model

- $h_p/L_c=0.01$
- - -  $h_p/L_c=0.05$
- - -  $h_p/L_c=0.10$
- - -  $h_p/L_c=0.25$

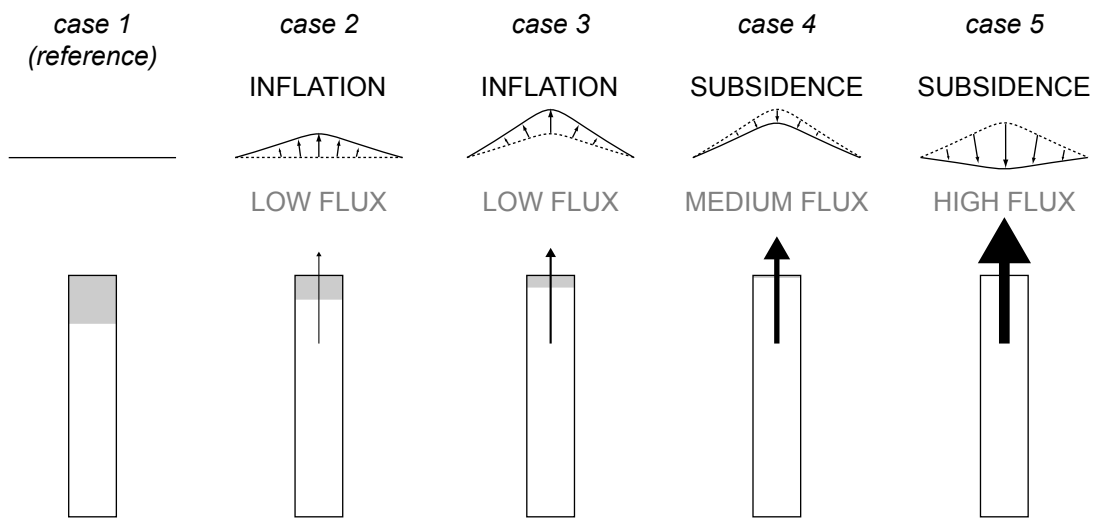
## Other models

- Sparks, 1997
- Collombet, 2009

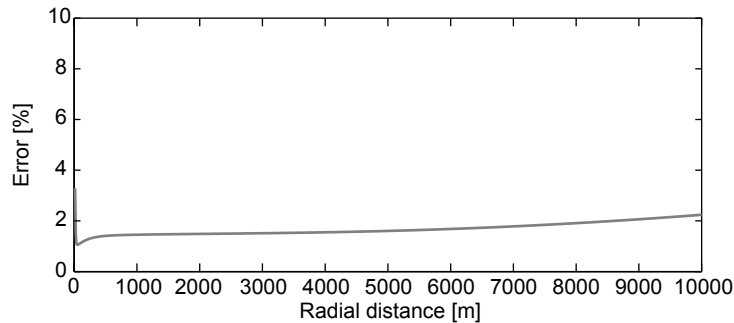
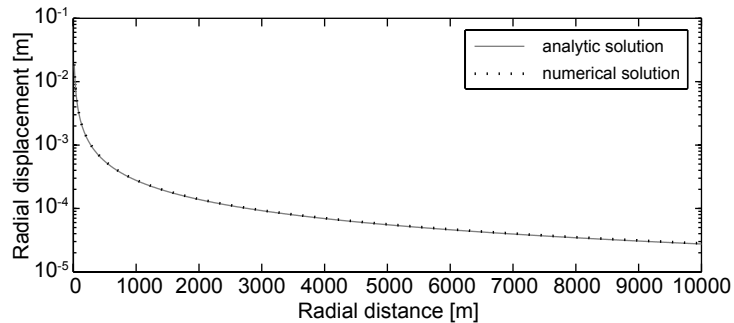
a)



b)



a)



b)

